

A Cold Atoms Apparatus for a New Hybrid Quantum System

by

Michelle Ann Sullivan

A thesis submitted in partial fulfillment of the requirements for the degree of

Master of Science

Department of Physics

University of Alberta

Abstract

As quantum computing research progresses, the need for a quantum network to allow communication between individual processors is becoming apparent. Such a network will require the ability to process, transmit, and store quantum information. Many quantum devices have been investigated, however individual devices are specialists in one task, and in order to realize a full-scale quantum network multiple devices will need to be combined into a hybrid quantum system (HQS).

This thesis describes efforts to construct a HQS which will combine laser-cooled atoms with other cryogenically-cooled quantum devices. The envisioned system requires the construction of a new apparatus where ^{87}Rb atoms will be laser cooled, then moved 60 cm into a dilution fridge where they will be coupled to other quantum devices. Once the apparatus is complete, we plan to conduct quantum memory, wavelength transduction, and state transfer experiments.

This work details the design of the ultra high vacuum chamber where the atoms will be laser cooled, as well as the optical set up required for the cooling. As well, simulations of the transport process are reported, and suggestions for possible transport schemes are given.

Preface

I set up the optics, as described in section 2.7.1 and 2.7.2. This set up was based off of the repump and cooling optics in our group's original system. Taras Hrushevskiy, Anindya Rastogi, and myself did the laser locking. Taras Hrushevskiy and James Chaulk build the electronics required for laser locking.

The atom cooling system design, described in chapter 3, was inspired by the system that already exists in our lab. I completed the design work for the apparatus described in this thesis with guidance and feedback from Dr. Lindsay LeBlanc, Dr. John P. Davis, and Greg Popowich. Myles Ruether and I made CAD drawings of the system. Myles Ruether and Taras Hrushevskiy designed the coil mounts. Taras Hrushevskiy, Myles Ruether, Greg Popowich, Brittany Lu, and myself cleaned and assembled the vacuum parts, and prepared the system for baking. James Chaulk wound the 2D and 3D MOT coils, and the bias coils.

Finally, I wrote the code to do the calculation found in the atom transport section, and did the calculations with guidance from Dr. Lindsay LeBlanc.

To my brother Robert

Acknowledgements

I would like to thank a number of people, without whom my success in the project would not be possible.

First, thanks to my supervisor Dr. Lindsay LeBlanc for her patience and guidance over the past two years.

I would also like to thank my lab mates for their for their willingness to answer questions and to occasionally assist with tasks in the lab. A special thanks goes to Logan Cooke for enlightening discussions about coding, to Ben Smith for welcoming me to the lab and taking time to patiently explain how things work, and to Brittany Lu who was always around to talk.

I want to extend a huge thanks to my family, especially my parents, for their support, encouragement, and unconditional love.

Thank you to all of my friends who provided much needed laughs and memories. I am grateful for the support and encouragement I have received from all of you.

And finally, I would like to thank Sourav Sarkar, who has made even the worst days more bearable.

Contents

1	Introduction	1
1.1	Motivation	1
1.2	Our Hybrid Quantum System	4
2	Laser Cooling	5
2.1	Doppler Cooling	5
2.1.1	The Two Level Atom	5
2.1.2	Scattering Force	6
2.1.3	Optical Molasses	8
2.1.4	The Doppler Limit	10
2.2	Sub-Doppler Cooling	11
2.2.1	σ^+/σ^- polarization	11
2.2.2	Lin/Lin-Polarization (Sisyphus cooling)	12
2.3	Magneto-Optical Traps	14
2.4	Optical Dipole Traps	15
2.5	Magnetic Trapping	19
2.6	Evaporative Cooling	20
2.7	Our Cooling/Trapping Procedure	21
2.7.1	Repump Optics	22
2.7.2	Cooling Optics	23
3	Apparatus	29
3.1	Design	29
3.1.1	Dispenser Region	29
3.1.2	2D-MOT Region	32

3.1.3	3D-MOT Region	33
3.2	Cleaning, assembly, and bakeout	36
4	Atom Transport	38
4.0.1	Theory: Moving ODT	38
4.1	Results	40
4.1.1	Calculations	40
4.1.2	Temperature Control	43
4.1.3	Simulations	43
5	Conclusion	56
	Appendix A Focus Tunable Lens Transport Code	64
	Appendix B Atom Distribution Generation Code	68
	Appendix C Atom Transport Simulation Code	72

List of Tables

3.1	The dimensions of each set of bias coils, along with the magnetic field that they produce.	35
4.1	Table summarizing the minimum transport times required for each velocity profile.	52

List of Figures

2.1	The populations of the ground state, ψ_1 , and the excited state, ψ_2 , vs. Ωt for various detunings.	7
2.2	Cartoon of the Doppler cooling mechanism.	9
2.3	The polarization gradient created by two interfering beams with opposite sigma polarization.	11
2.4	The cooling scheme for Lin/Lin (Sisyphus) cooling.	12
2.5	Diagram of magneto-optical trap operation in one-dimension.	14
2.6	Plots showing the concept of evaporative cooling.	20
2.7	Hyperfine structure on the ^{87}Rb D_2 line including the transitions used in our experiment.	25
2.8	Legend of optical components.	26
2.9	Repump optics set-up.	27
2.10	Cooling optics set-up.	28
3.1	CAD drawing of the full apparatus.	30
3.2	CAD drawing of the cold-atoms UHV system.	31
3.3	CAD drawing of the cold-atoms system, with optics and coils mounted.	35
4.1	Plots showing the potential and scattering rate in an optical dipole trap.	41
4.2	Plots of the transport beam in the initial and final positions.	42
4.3	Velocity and momentum distributions of the atoms used in the transport simulation.	46
4.4	Position, velocity, and acceleration for the Gaussian velocity profile.	48

4.5	Simulation results using the Gaussian trap velocity profile. . .	49
4.6	Position, velocity, and acceleration for the triangular velocity profile.	50
4.7	Simulation results using a triangular trap velocity profile. . . .	53
4.8	Position, velocity, and acceleration, for the sine-squared velocity profile.	54
4.9	Simulation results using the sine-squared trap velocity profile.	55

Chapter 1

Introduction

1.1 Motivation

In 1982 Richard Feynman proposed that to simulate nature, which is quantum mechanical, we need a computer that is made of quantum elements [1]. Since then, interest in quantum computers has grown rapidly. These computers use algorithms that would not be possible with classical computers, providing increased problem solving capabilities. Algorithms which offer the possibility to outperform classical computers have been developed, such as Shor's algorithm [2], which has security implications for RSA encryption. Quantum computing and quantum information is an active area of current research, with efforts ranging from preliminary fundamental research, to companies such as IBM, D-wave Systems, and Honeywell, who are working towards developing large-scale quantum processors, to Google's (albeit disputed [3,4]) result showing quantum "supremacy" [5]. There have been many proposals for areas of research that could be accelerated by these powerful computers including, but not limited to drug discovery [6], high-energy physics [7], medical image reconstruction [8], traffic flow optimization [9], and protein folding simulations [10]. Quantum computation is an exciting area of research, where many exciting and probably unexpected developments will take place in the years to come.

Although quantum computers themselves are novel and exciting quantum technologies, research efforts extend beyond processing quantum information and solving hard problems. Just as the power of classical computers has been

increased by joining them together and allowing them to communicate via the internet, a “quantum internet” that allows quantum computers to communicate with one another would increase the power of individual quantum processors [11]. This type of “quantum communication” would require the ability to transmit the quantum bits, or “qubits” which process the quantum information [12]. For a full communications network, the ability to coherently transfer states between light and matter [11], as well as the ability to store states in a quantum memory are also desirable.

To date, many individual quantum systems have been studied, including cold atoms and ions [13], superconducting qubits [14], mechanical resonators [15], microwave and optical cavities [16], spin systems [17], and quantum dots [18]. Each of these systems is interesting on its own, however they are specialists; each is good for one specific task. For example, superconducting qubits can quickly process quantum information, but have short coherence times making them a poor storage platform. In contrast, ultracold atoms experience minimal thermal fluctuations and are isolated from their environment, resulting in long coherence times, making them ideal for memory applications [19]. Although we have the capabilities to process, store, and transmit quantum information there is no device that can do all of these tasks at the same time [19], making communications via a quantum internet appear out of reach. Enter the hybrid quantum system (HQS). A HQS would combine multiple quantum devices, each fulfilling a role to which it is well suited, into a larger device capable of performing multiple tasks simultaneously [19]. Although this may sound straightforward, in reality the realization of the HQS is a difficult task. Not all quantum systems interface with one another, and many operate in different, often extreme and difficult to create, environments, such as cryogenic temperatures, or ultrahigh vacuum. We aim to build a new and versatile apparatus that will allow us to combine laser-cooled atoms with cryogenically-cooled devices in a dilution refrigerator.

Much research into atomic hybrid quantum systems has already taken

place. Although not an exhaustive list, some examples include a proposal to couple solid-state qubits to atoms [20], a study of how the presence of a superconducting ring close to an atom trap modifies the trapping potential [21], and the realization of on-chip systems combining cold atoms and a superconducting coplanar waveguide resonator [22, 23].

In order to create a system with greater versatility, it is desirable to prepare cold atoms in one location and to later move them closer to the device under investigation, where they can be trapped on a stand-alone atom chip [24]. Preparing the atoms separate from the other device allows multiple devices to be studied without fabricating additional atom chips [24]. Additionally, as the atoms are cooled in a separate location, changing samples will not require the cooling optics to be re-aligned [24]. A 2013 paper by Naides *et al.* demonstrated such a system using a two-chamber apparatus [24]. Atoms were cooled in one chamber before being optically transported into another chamber, where they were magnetically trapped in proximity to another device. The other device is held on a cold finger and is cooled with liquid nitrogen. Work has also been done on a system that allows cold atoms to be moved into the 4K stage of a dilution fridge for further experimentation [25].

Many quantum devices require temperatures below liquid nitrogen (77 K) and liquid ^4He (4 K) cooling. Using a dilution fridge capable of reaching millikelvin temperatures is necessary for devices such as superconducting qubits to operate at their full potential [26]. To date, a few groups have demonstrated such a system. J. Fortágh's group was able to prepare cold atoms in the 6 K stage of a dilution fridge and to magnetically transport them to the millikelvin stage where they would be coupled to devices cooled to millikelvin temperatures [26]. Another similar apparatus designed to couple ultracold atoms to superconducting devices has recently been built by a group in Singapore [27]. This apparatus distinguishes itself from the former by preparing the atoms outside of the dilution fridge, before magnetically transporting them to the millikelvin stage. A German group has built an apparatus where a lattice of

laser-cooled atoms are held in a chamber outside of a dilution fridge and coupled via light to a mechanical membrane located inside a dilution fridge [28]. They claim that by using a combination of feedback and sympathetic cooling they will be able to realize coupling between both systems in their ground state [29].

1.2 Our Hybrid Quantum System

We have designed a hybrid quantum system that combines laser-cooled atoms and cryogenically-cooled components. Cold atoms will be prepared in an ultrahigh vacuum chamber using laser cooling. The chamber is connected to a dilution fridge via a flexible bellows, allowing the atoms to be moved between the preparation chamber and the fridge. Once in the fridge, the atoms can be captured and coupled to the quantum devices which operate inside the fridge. The exact capture method is yet to be decided, but at this point we are considering an on-chip magnetic trap. A gate valve will separate the cold atoms preparation chamber and fridge, allowing the macroscopic quantum system to be exchanged without the need for baking the cold atoms preparation portion. In addition, this feature will allow the two systems to operate independently if desired.

The goal of this system is to couple cold atoms to other quantum systems in order to perform state transfer, wavelength transduction, quantum memory, and quantum computation. At this point there are no firm plans for the experiments, although we are currently investigating microwave to optical wavelength transduction using atoms in a cryogenically-cooled microwave cavity.

Details of the laser-cooling procedure are given in section section 2, the apparatus used to prepare the cold atoms is described in section 3, and the transport system is discussed in section 4.

Chapter 2

Laser Cooling

At the center of our experiment lie confined clouds of laser-cooled atoms. Cooling and trapping atoms is a complicated process, which requires many steps and a complex set-up. In this chapter the theory behind cooling atoms is explained, and our cooling and trapping procedure, as well as the optical set-up, is described.

2.1 Doppler Cooling

2.1.1 The Two Level Atom

Interactions between the atom and incoming light will be explained in the semi-classical picture where the atom is treated quantum-mechanically, and can be approximated as a two-level system. The incoming radiation is treated as a classical oscillating electric field, $\mathbf{E} = \mathbf{E}_0 \cos(\omega t)$, where ω is the radiation frequency. The interaction between the atom and the radiation can be described as a perturbation to the base Hamiltonian, H_0 , by an interaction Hamiltonian term

$$H_I(t) = e\mathbf{r} \cdot \mathbf{E}_0 \cos(\omega t), \quad (2.1)$$

where \mathbf{r} gives the atomic electron's position from the atomic center of mass. Written in the basis states of the unperturbed Hamiltonian, which satisfy $H_0\psi_n(\mathbf{r}) = E_n\psi_n(\mathbf{r})$, $n = 1, 2$, the wavefunction for this system is

$$\Psi(\mathbf{r}, t) = c_1(t)\psi_1(\mathbf{r})e^{-iE_1t/\hbar} + c_2(t)\psi_2(\mathbf{r})e^{-iE_2t/\hbar}, \quad (2.2)$$

where $c_1(t)$ and $c_2(t)$ satisfy $|c_1(t)|^2 + |c_2(t)|^2 = 1$.

When $\Psi(\mathbf{r}, t)$ is used in the time-dependent Schrodinger equation,

$$i\hbar \frac{\partial \Psi}{\partial t} = (H_0 + H_I)\Psi, \quad (2.3)$$

we end up with two coupled differential equations [30]:

$$i\dot{c}_1(t) = \Omega \cos(\omega t) e^{-i\omega_0 t} c_2(t) \quad (2.4)$$

and

$$i\dot{c}_2(t) = \Omega^* \cos(\omega t) e^{i\omega_0 t} c_1(t), \quad (2.5)$$

where $\omega_0 = \frac{E_2 - E_1}{\hbar}$ is the atomic resonance frequency, and $\Omega = \frac{\langle 1 | \mathbf{e} \cdot \mathbf{E}_0 | 2 \rangle}{\hbar}$ is the Rabi frequency. If we assume that initially all of the population is in the lower level, $|c_1(t)|^2 = 1$, and invoke the rotating wave approximation (assume the $e^{-i(\omega+\omega_0)}$ terms average to zero) we find that [30]

$$|c_2(t)|^2 = \frac{\Omega^2}{(\Omega^2 + \delta^2)} \sin^2\left(\frac{\sqrt{\Omega^2 + \delta^2} t}{2}\right). \quad (2.6)$$

In the resonant case $\omega = \omega_0$, $\delta = 0$, and we find that

$$|c_2(t)|^2 = \sin^2\left(\frac{\Omega t}{2}\right) \quad (2.7)$$

and the population oscillates between ψ_1 and ψ_2 with period $\frac{1}{2\Omega}$. As the frequency of the incoming light moves further from resonance the oscillation period decreases, and a smaller fraction of atoms are able to reach the excited state, ψ_2 . This is shown in figure 2.1.

The above only considered the interaction of the atoms with an external electric field. The atoms can also spontaneously emit photons and decay from the excited state to the ground state. This is quantified by Γ , the natural linewidth of the transition. Γ^{-1} gives the lifetime of the excited state.

2.1.2 Scattering Force

Light carries momentum, and when it scatters off of a surface, it will impart momentum onto that object. This is seen when light is absorbed and

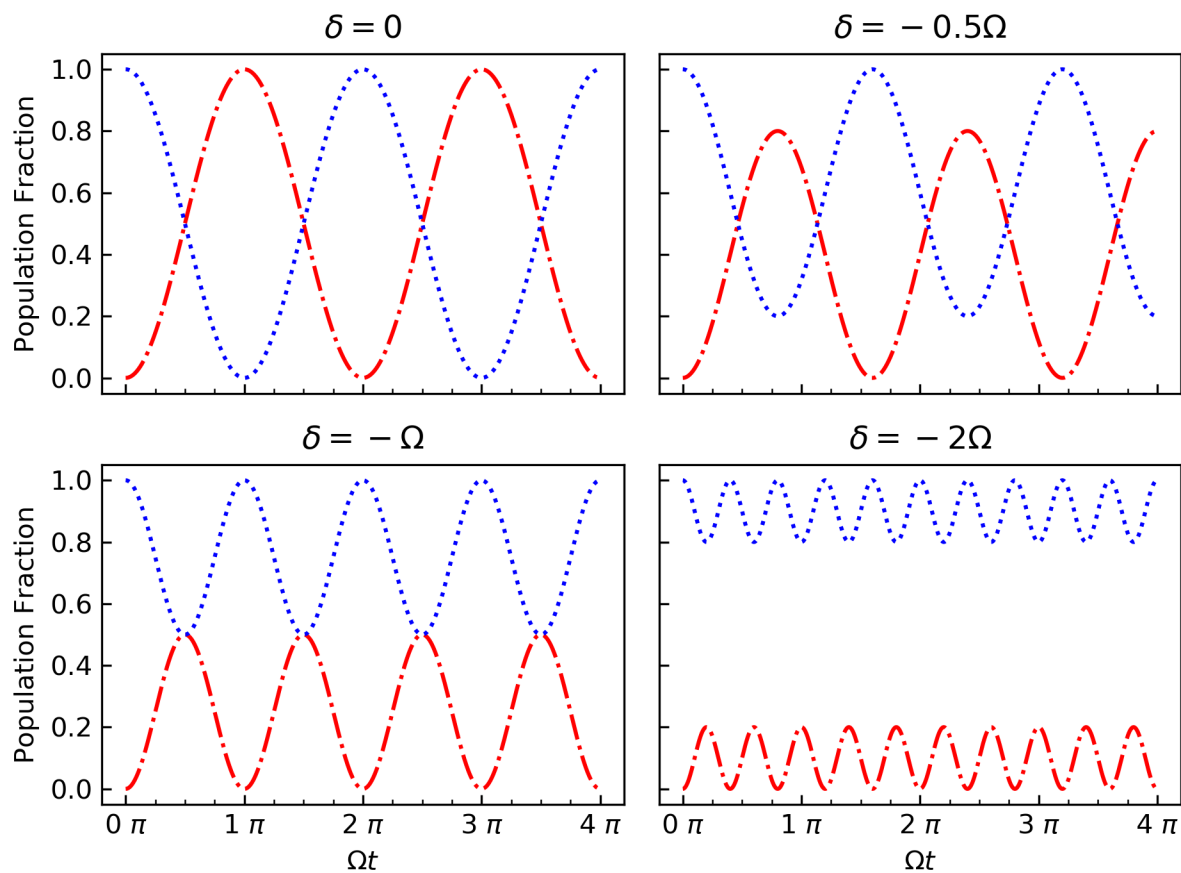


Figure 2.1: The populations of the ground state, ψ_1 , and the excited state, ψ_2 , vs. Ωt for various detunings. The blue dotted line shows $|c_1(t)|^2$ and the red dash-dotted line shows $|c_2(t)|^2$. At zero detuning, δ (top left) full population transfer occurs when $\Omega t = \pi$. As the detuning increases the fraction of atoms transferred into the excited state decreases, and the period increases. For $\delta = -2\Omega$ only $1/5$ of the ground state population can be excited and maximum transfer occurs when $\Omega t = \frac{2\pi}{5}$ (bottom right).

re-emitted by atoms. The force on an atom that absorbs a photon with momentum $\hbar\mathbf{k}$ is given by:

$$\mathbf{F}_{\text{sc}} = \left\langle \frac{d\mathbf{p}}{dt} \right\rangle = \hbar\mathbf{k} \left\langle \frac{1}{\Delta t} \right\rangle = \hbar\mathbf{k} \Gamma_{\text{sc}}, \quad (2.8)$$

where $\Gamma_{\text{sc}} = \Gamma\rho_{22}$ is the scattering rate, where Γ is the transition natural line width, and ρ_{22} is the population fraction in the excited state. ρ_{22} is given by [30]:

$$\rho_{22} = \frac{\Omega/4}{\delta^2 + \Omega^2/2 + \Gamma^2/4}, \quad (2.9)$$

where Ω is the Rabi frequency describing the light-induced transfer between the ground and excited states, and δ is the detuning. Using the ratio of the intensity of incoming light, I , to the saturation intensity, I_{sat} , $I/I_{\text{sat}} = 2\Omega^2/\Gamma^2$, we can combine (2.8) and (2.9) to find that the scattering force is [30]

$$\mathbf{F}_{\text{sc}} = \hbar\mathbf{k} \frac{\Gamma}{2} \frac{I/I_{\text{sat}}}{1 + I/I_{\text{sat}} + 4\delta^2/\Gamma^2}. \quad (2.10)$$

2.1.3 Optical Molasses

Cooling atoms using radiation was first proposed in 1975 [31]. To understand this technique, consider an atom moving with a velocity \mathbf{v} . As it moves towards a laser beam, the Doppler shift will kick in. If the the light is red-detuned (frequency below resonance), an atom moving towards it will see the light Doppler shifted closer to resonance. When the atom absorbs, it will get a momentum kick in the direction opposite to its motion, slowing it down. Assuming the light intensity is below saturation, the photon will be spontaneously re-emitted in a random direction. Since re-emission is random, the momentum kicks from re-emission will average to zero. The process is shown in figure 2.2

Assume there are two counter-propagating beams. The net force felt by a moving atom is the difference between the scattering forces in each direction,

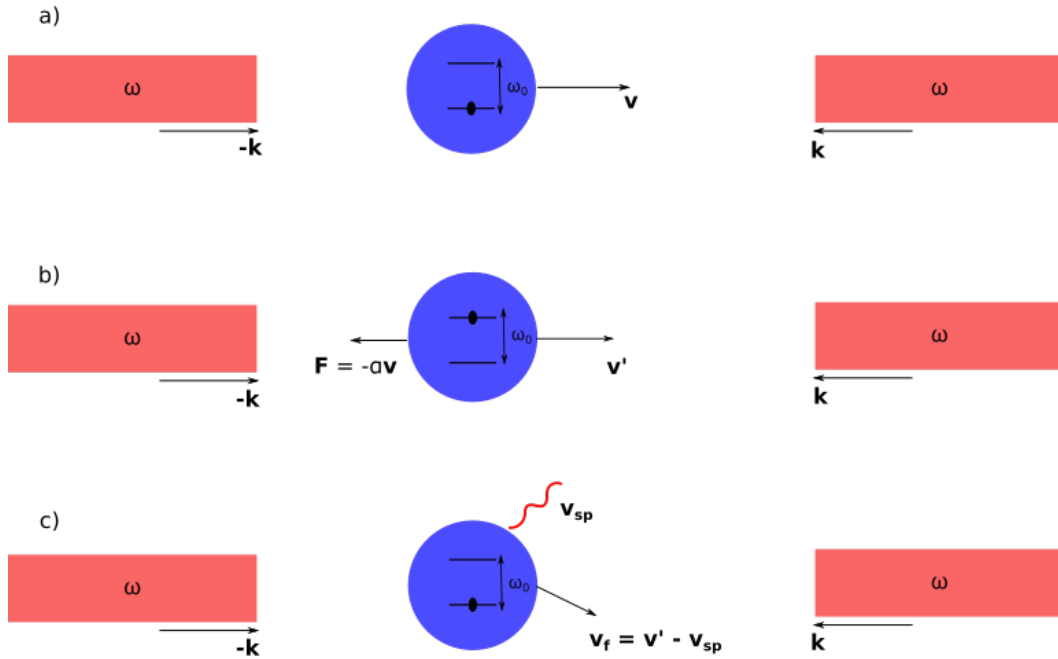


Figure 2.2: Cartoon of the Doppler Cooling mechanism. The atom is modeled as a two-level system. a) An atom in the ground state moves towards a red-detuned laser beam, frequency ω , with velocity \mathbf{v} . b) When $\omega - \omega_0 = \mathbf{k} \cdot \mathbf{v}$ the atom absorbs, and transitions to the excited state. The atom feels a force $\mathbf{F} = -a\mathbf{v}$ in the direction opposite to its motion, slowing it to $\mathbf{v}' < \mathbf{v}$. c) The atom spontaneously emits a photon, returning to the ground state. It will continue with velocity $\mathbf{v}_f = \mathbf{v}' - \mathbf{v}_{sp}$. When the absorption and re-emission process occurs for many atoms, the \mathbf{v}_{sp} components average to zero, resulting in a net cooling.

$$\mathbf{F}_{\text{net}} = \mathbf{F}_{\text{sc}}(\delta + \mathbf{k} \cdot \mathbf{v}) - \mathbf{F}_{\text{sc}}(\delta - \mathbf{k} \cdot \mathbf{v}):$$

$$\begin{aligned} \mathbf{F} &= \frac{\hbar \mathbf{k} \Gamma I}{2I_{\text{sat}}} \left[\frac{1}{1 + \frac{I}{I_{\text{sat}}} + \frac{4(\delta + \mathbf{k} \cdot \mathbf{v})^2}{\Gamma^2}} - \frac{1}{1 + \frac{I}{I_{\text{sat}}} + \frac{4(\delta - \mathbf{k} \cdot \mathbf{v})^2}{\Gamma^2}} \right] \\ &= \frac{\hbar \mathbf{k} \Gamma I}{2I_{\text{sat}}} \frac{8\delta \mathbf{k} \cdot \mathbf{v} / \Gamma^2}{(1 + I/I_{\text{sat}} + 4(\delta + \mathbf{k} \cdot \mathbf{v})^2/\Gamma^2)(1 + I/I_{\text{sat}} + 4(\delta - \mathbf{k} \cdot \mathbf{v})^2/\Gamma^2)} \end{aligned} \quad (2.11)$$

If the Doppler shift is much less than the natural linewidth ($|\mathbf{k} \cdot \mathbf{v}| \ll \Gamma$), we have:

$$\mathbf{F} = -\frac{8I\hbar k^2 \delta \mathbf{v}}{\Gamma I_{\text{sat}} (1 + I/I_{\text{sat}} + 4\delta^2/\Gamma^2)^2} = -a\mathbf{v}, \quad (2.12)$$

where a is given by

$$a = 4\hbar k^2 \frac{I}{I_{\text{sat}}} \frac{-2\delta/\Gamma}{[1 + I/I_{\text{sat}} + 4\delta^2/\Gamma^2]^2}. \quad (2.13)$$

This force is proportional to the velocity, much like viscosity. It is referred to as “optical molasses”, referencing the fact that molasses is a viscous fluid.

2.1.4 The Doppler Limit

There is a fundamental limit to the Doppler cooling mechanism. Although the momentum kicks from the emitted photons average to zero, there will be a small net displacement in the direction of the beam (this is similar to Brownian motion) [30]. There is a Poissonian variation in the number of photons absorbed and emitted in a time t , which results in an additional random walk [30]. Both of these effects oppose the “viscous” force acting on the atoms, and result in heating. This places a limit on the temperature that can be reached by molasses cooling. Assuming that the intensity is below the saturation intensity, this temperature is given as a function of the detuning, δ , and the natural linewidth, Γ , as [30]

$$T(\delta) = \frac{\hbar \Gamma}{4k_B} \frac{1 + (2\delta/\Gamma)^2}{2|\delta|/\Gamma}. \quad (2.14)$$

This temperature is a function of delta, and will have a minimum for some value of delta given by

$$\frac{dT}{d\delta} = \left(\frac{-\hbar \Gamma^2}{8k_B} \right) \left(\frac{-1}{\delta^2} + \frac{4}{\Gamma^2} \right) = 0. \quad (2.15)$$

Using (2.15), we find that the temperature has a minimum value at $\delta = -\frac{\Gamma}{2}$. We can use this value in (2.14) to find that the minimum temperature allowed by Doppler cooling is

$$T_D = \frac{\hbar\Gamma}{2k_B}. \quad (2.16)$$

For ^{87}Rb , $\Gamma = 2\pi \cdot 6.056 \text{ MHz}$ [32], which gives a Doppler temperature of $140 \mu\text{K}$.

2.2 Sub-Doppler Cooling

When the first laser-cooling experiments were conducted, it was found that temperatures well below the Doppler limit could be achieved [33]. This is due to the fact that atoms are not an ideal two-level system; they actually have a complicated structure of sub-levels. Two of the mechanisms behind this phenomenon are outlined below.

2.2.1 σ^+/σ^- polarization

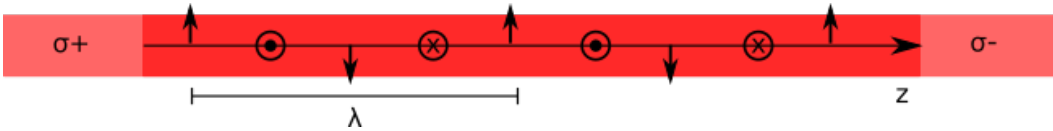


Figure 2.3: When counter-propagating beams with opposite circular polarization interfere they create a linear polarization gradient that rotates with a period equal to the wavelength of light.

When two counter-propagating beams with opposite circular polarization interfere, they create a standing wave with a linear polarization that rotates with a period of the laser wavelength, λ , as seen in figure 2.3. This results in a motion-induced atomic orientation, and as a result the atoms will absorb preferentially from the beam towards which it travels, resulting in a damping force more efficient than the one in Doppler cooling [34].

Consider an atom in the $F = 1$ ground state at rest, and take the quantization axis to be the direction of polarization. The ground state will be split into m_F sub-levels with $m_f = 0, \pm 1$. The $m_F = 0$ sublevel will have a larger

population than the $m_F = \pm 1$ states as this is the stronger π -transition. Now assume that when the atom moves in the z -direction it is moving towards the σ^- beam. If the beam is red-detuned, when we work in a frame rotating with the polarization gradient there will be more atoms in the $m_F = -1$ ground state than in the $m_F = 1$ state [34], and the atom will absorb light from the σ^- beam with 6 times greater probability than the σ^+ beam. Similarly, atoms moving along $-z$, towards the σ^+ beam, will have a greater population in the $m_F = 1$ ground state, and there is greater probability that the atom absorbs from the σ^+ beam. This results in an unbalanced force, which damps the motion of the atom.

2.2.2 Lin/Lin-Polarization (Sisyphus cooling)

In addition to the sub-Doppler mechanism that is generated by circularly-polarized light, there are additional effects caused by counter-propagating beams with orthogonal linear polarization. Although we use circularly-polarized beams for our experiment, we use light in 3-dimensions, resulting in a complex polarization pattern, and $\text{lin} \perp \text{lin}$ cooling comes into play.

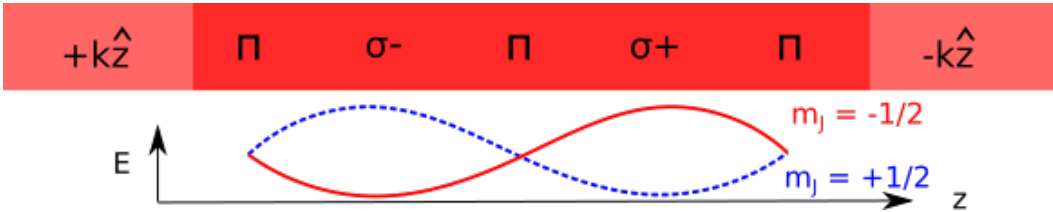


Figure 2.4: When counter-propagating beams with opposite linear polarization interfere they create a standing wave pattern that rotates between linear and circular polarization. Due to the AC Stark shift, the energy of the $m_j = \pm \frac{1}{2}$ sublevels shifts depending on the polarization. Adapted from [30].

The result of counter-propagating orthogonal linear beams is a standing wave pattern where the polarization rotates between linear and circular polarization, as seen in figure 2.4. Consider a two-level atom, with ground state $J = \frac{1}{2}$ and excited state $J = \frac{3}{2}$. The ground and excited states will be split into m_J sub-levels with $-J < m_J < J$. Consider a region of σ^+ polarization. With

σ^+ polarized light there are two ground to excited state transitions which satisfy the $\Delta M_J = 1$ selection rule: $M_J = -\frac{1}{2} \rightarrow M_J = \frac{1}{2}$ and $M_J = \frac{1}{2} \rightarrow M_J = \frac{3}{2}$. Since the transition strength is stronger for the $M_J = \frac{1}{2} \rightarrow M_J = \frac{3}{2}$ transition (Clebsch-Gordan coefficient of 1, vs. $\sqrt{\frac{1}{3}}$ for the $M_J = -\frac{1}{2} \rightarrow M_J = \frac{1}{2}$ transition) the atoms will be optically pumped into the $M_J = \frac{1}{2}$ ground state [34]. Due to the AC Stark effect, the ground state sub levels will have an energy shift downward, with the shift for the $M_J = \frac{1}{2}$ sub level being greater because it is a stronger transition. Following the same argument, in a σ^- region atoms will be optically pumped in the $M_J = -\frac{1}{2}$ ground state sub level, and this level will also see an energy shift below the $M_J = \frac{1}{2}$ sub level.

Let's look at the above process more closely to see how it results in cooling of atoms. As the atom moves in space it sees rotating polarization, causing the energy levels to shift up and down in a sinusoidal pattern. As the atoms move in space, they have to "climb" hills, converting kinetic energy to potential energy [34]. Once at the top of a hill, the atom will be excited into the $J' = \frac{3}{2}$ state, however, when it spontaneously emits a photon and transitions back to the ground state it is more likely to fall into the lower ground state sub-level (this is known as "optical pumping") [34]. For example, if an atom in the $M_J = -\frac{1}{2}$ state absorbs a σ^+ photon at a potential maximum and transitions into the $M'_J = \frac{3}{2}$ excited it will have a higher probability to spontaneously emit into the lower energy $M_J = \frac{1}{2}$ ground state. This process requires a higher energy photon than was absorbed. Physically this means that the additional potential energy gained when climbing the hill is carried away with the photon, leaving the atoms with less kinetic energy, thus cooling it [34].

The theoretical limit on the temperature that can be reached through this mechanism is set by the recoil energy from spontaneous emission [30], and is given by:

$$T = \frac{h^2}{mk_B\lambda^2}, \quad (2.17)$$

where h is Plank's constant, m is the mass of a ^{87}Rb atom, k_B is the Boltzmann

constant, and λ is the light's wavelength.

2.3 Magneto-Optical Traps

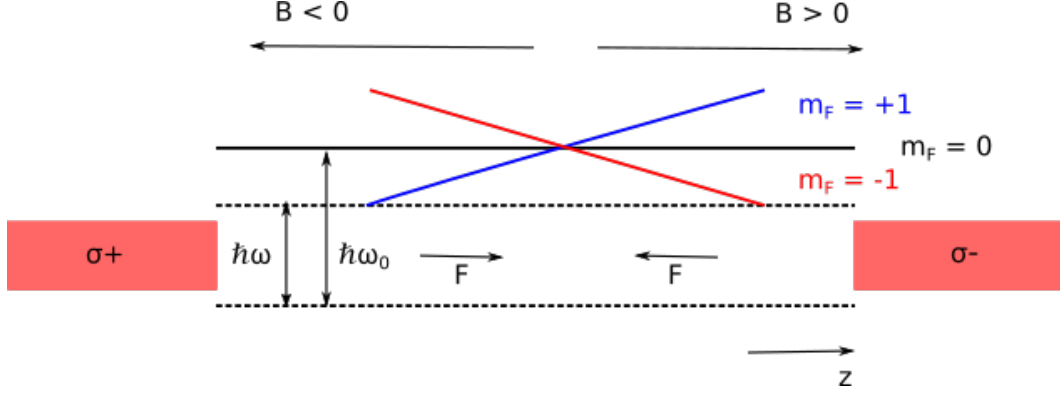


Figure 2.5: Schematic showing a magneto-optical trap in 1 dimension. As atoms move along the magnetic field gradient their Zeeman sub-levels are shifted into resonance with the red-detuned beam, creating a position-dependent force which pushed them towards the center of the trap.

The force the atoms experience in Doppler cooling slows them down, but this force does not depend on position, therefore atoms will eventually diffuse out of the cooling region. Using a set of anti-Helmholtz coils to create a magnetic field gradient can create a magneto-optical trap (MOT) for atoms [35].

First consider the one-dimensional case shown in figure 2.5, where 2 red-detuned, counter-propagating beams have opposite circular polarization (σ^+ and σ^-). Due to the external magnetic field, the energy levels in the atoms are Zeeman shifted, and there is an additional term in the detuning,

$$\omega_Z = \frac{\mu' B}{\hbar}, \quad (2.18)$$

where

$$\mu' = g_F m_F \mu_B. \quad (2.19)$$

In (2.19) m_f is the Zeeman sub-level, μ_B is the Bohr magneton, and g_F is given by

$$g_F = \frac{F(F+1) + J(J+1) - I(I+1)}{2F(F+1)} g_J, \quad (2.20)$$

where J is the quantum number describing total angular momentum, I is the quantum number for nuclear spin, $\mathbf{F} = \mathbf{I} + \mathbf{J}$, and

$$g_J = \frac{3}{2} + \frac{S(S+1) - L(L+1)}{2J(J+1)}, \quad (2.21)$$

where S is the spin quantum number, and L is the angular momentum quantum number.

Now the total detuning, δ' , is,

$$\delta' = \delta + \omega_D + \omega_Z. \quad (2.22)$$

Since the magnetic field, $B(z)$, depends on the position, atoms will experience a position-dependent detuning. Here we assume the magnetic field gradient is linear, and that the field is zero at $z = 0$. As an atom moves towards the σ^- beam in the $+z$ direction, the $m_F = 1$ state is shifted to higher energy, away from resonance, and the $m_F = -1$ state will be shifted to lower energy, closer to resonance with the red-detuned beam. If the atom moves towards the σ^+ beam, it will absorb, and be pushed towards the centre of the trap. A similar process will take place when atoms moving in the $-z$ direction see the $m_F = 1$ level shifted to resonance with the σ^+ beam. This process cools the atoms by slowing them down and confines the atoms by pushing them towards the centre of the trap. This can be extended to three dimensions by using 3 orthogonal sets of counter-propagating beams and a 3-dimensional field gradient provided by a set of coils in the anti-Helmholtz configuration.

2.4 Optical Dipole Traps

Once we have cooled the atoms, we may wish to confine them, or to transport them to another location. Light can create a dipole force, which can be used to trap atoms. The dipole force on an atom in an external electromagnetic field can be understood by approximating the atom as a driven/damped

harmonic oscillator. In this picture, an electron is bound to the core of the atom, and it oscillates at the resonance frequency, ω_0 [36]. The electric field, $\mathbf{E}(r, t) = \mathbf{E}(r)e^{-i\omega t} + c.c.$, drives the oscillations with frequency ω , and causes the atom to acquire an atomic dipole moment, $\mathbf{p} = \alpha\mathbf{E}$, where α is the complex polarizability. We also assume that the electric field is uniform over the size of an atom, and neglect the r dependence. The motion of the electron is described by

$$\ddot{x} + \Gamma_\omega \dot{x} + \omega_0^2 x = \frac{eE(t)}{m_e}, \quad (2.23)$$

where Γ_ω is the radiative lifetime, and m_e is the mass of the electron. Using x in the form $x(t) = x_0 e^{-i\omega t}$, we find that the solution to (2.23) is

$$x_0 = \frac{eE}{m_e} \frac{1}{\omega_0^2 - \omega^2 - i\Gamma_\omega \omega}. \quad (2.24)$$

We can find the polarizability from (2.24) by using the fact that $\vec{p} = -e\vec{x} = \alpha\vec{E}$. This gives

$$\alpha = \frac{e^2}{m_e} \frac{1}{\omega_0^2 - \omega^2 - i\Gamma_\omega \omega}. \quad (2.25)$$

Next, we can consider that the classical radiative lifetime, Γ_ω , is given by [30]

$$\Gamma_\omega = \frac{e^2 \omega^2}{6\pi\epsilon_0 m_e c^3}, \quad (2.26)$$

where ϵ_0 is the permittivity of free space, and c is the speed of light.

We can use (2.26), along with the fact that the the resonant damping rate is given by $\Gamma = \frac{\omega_0^2}{\omega^2} \Gamma_\omega$ to rewrite α as

$$\alpha = 6\pi\epsilon_0 c^3 \frac{\frac{\Gamma}{\omega_0^2}}{\omega_0^2 - \omega^2 - i(\frac{\omega^3}{\omega_0^2})\Gamma}. \quad (2.27)$$

For strong dipole-allowed transitions, such as the D lines in ^{87}Rb , the natural linewidth of the transition is a good approximation to Γ [36]. It should also be noted that the above is a classical approximation, however, we are dealing with a quantum-mechanical system. Quantum-mechanical systems introduce the possibility of saturation. Optical dipole traps use light which is far detuned from the atomic transition, therefore saturation is negligible, and the

classical case is a reasonable approximation [36].

Next, consider the potential resulting from the interaction of the induced dipole with an external field which has an intensity profile $I = 2\epsilon_0 c |\mathbf{E}|^2$,

$$U_{\text{dip}} = -\frac{1}{2} \langle \mathbf{p} \mathbf{E} \rangle = -\frac{1}{2\epsilon_0 c} \text{Re}(\alpha) I(r), \quad (2.28)$$

where the real component of the polarizability corresponds to the in-phase component of the oscillations and thus contributes to the force. In contrast, the imaginary component is out-of-phase and contributes to the optical dispersion. We can determine the corresponding dipole force by taking the gradient of this potential

$$\mathbf{F}_{\text{dip}}(r) = -\nabla U_{\text{dip}}(r) = \frac{1}{2\epsilon_0 c} \text{Re}(\alpha) \nabla I(r). \quad (2.29)$$

The atom can also absorb power from the driving field, which will then be re-emitted as photons. This results in a scattering process, with a rate which depends on the absorbed power:

$$\Gamma_{\text{sc}} = \frac{P_{\text{abs}}}{\hbar\omega} = \frac{1}{\hbar\epsilon_0 c} \text{Im}(\alpha) I(r). \quad (2.30)$$

We can use equation (2.27) for the complex polarizability in equations (2.28) and (2.30) to find

$$U_{\text{dip}}(r) = \frac{3\pi c^2}{2\omega_0^2} \left(\frac{\Gamma}{\omega_0 - \omega} + \frac{\Gamma}{\omega_0 + \omega} \right) I(r), \quad (2.31)$$

and

$$\Gamma_{\text{sc}}(r) = \frac{3\pi c^2}{2\hbar\omega_0^3} \left(\frac{\omega}{\omega_0} \right)^3 \left(\frac{\Gamma}{\omega_0 - \omega} + \frac{\Gamma}{\omega_0 + \omega} \right)^2 I(r). \quad (2.32)$$

We can define the detuning as $\delta = \omega - \omega_0$. If we assume that $|\delta| \ll \omega_0$, we can make the rotating wave approximation, which gives:

$$U_{\text{dip}}(r) = \frac{3\pi c^2}{2\omega_0^3} \frac{\Gamma}{\delta} I(r), \quad (2.33)$$

and

$$\Gamma_{\text{sc}}(r) = \frac{3\pi c^2}{2\hbar\omega_0^3} \left(\frac{\Gamma}{\delta} \right)^2 I(r). \quad (2.34)$$

Equations (2.33) and (2.34) illustrate two important features of optical dipole traps. First, the sign of the potential depends on the sign of the detuning. If the light is red detuned ($\delta < 0$), the potential minimum will be in regions of high intensity. In other words, atoms will be attracted to intensity maxima. If light is blue detuned ($\delta > 0$) atoms will be repelled from intensity maxima. Second, the strength of the potential decreases as $1/\delta$ as the laser light moves away from atomic resonance. However, the scattering goes as $1/\delta^2$. Therefore, it is advantageous to use large detuning to reduce scattering, since scattering causes atoms to heat up and escape the trap.

Gaussian beams have an intensity profile which is maximum in the centre and decreases towards the edges:

$$I_G(r, z) = \frac{2P}{\pi w^2(z)} e^{-\frac{2r^2}{w^2(z)}}, \quad (2.35)$$

where

$$w(z) = w_0 \sqrt{1 + \left(\frac{z}{z_R}\right)^2}, \quad (2.36)$$

P is the laser power, w_0 is the beam waist, and z_R is the Rayleigh range which gives the distance over which the beam cross-section doubles.

A Gaussian beam will create an intensity gradient. We assume that the atoms have low thermal energy, and are confined to the bottom of the trap. Then, we can approximate the potential felt by the atoms as harmonic:

$$U(r, z) = U_0 - \frac{1}{2}m\omega_r^2 r^2 - \frac{1}{2}m\omega_z^2 z^2, \quad (2.37)$$

where U_0 is the trap depth (optical potential),

$$U_0 = \frac{3c^2 P \Gamma}{\omega_0^3 w_0^2 \delta}, \quad (2.38)$$

and $\omega_r = \sqrt{\frac{4U_0}{mw_0^2}}$ and $\omega_z = \sqrt{\frac{2U_0}{mz_r^2}}$ are the radial and axial frequencies, respectively.

2.5 Magnetic Trapping

Atoms in a magnetic field “see” their m_F energy levels shifted by an amount proportional to the magnitude of the magnetic field:

$$U = g_F \mu_B m_F |\mathbf{B}|. \quad (2.39)$$

This potential creates a force acting on the atoms:

$$\mathbf{F} = -\nabla U = -g_F \mu_B m_F \frac{d\mathbf{B}}{dz}. \quad (2.40)$$

For atoms in a state with $g_F m_F < 0$ the force increases with increasing field, and the atoms are attracted to regions with larger magnetic fields. For states with $g_F m_F > 0$ the force is greatest at low fields, and the atoms are attracted to a magnetic field minimum. This force can be used to trap atoms.

A magnetic field gradient can be created by using two coils in the anti-Helmholtz configuration. The magnetic field will be at a minimum at the centre of the coils, and increases linearly in the radial direction. Atoms in trappable states, $g_F m_F > 0$ will be trapped in the magnetic field minimum at the centre of the coils.

It is experimentally feasible to create large field gradients, and thus deep traps. However, problems arise near the centre of the trap where the magnetic field, and thus the spacing between Zeeman energy levels, is small. Noise, fluctuations in the field, and collisions can cause atoms to be transferred into untrappable energy levels, causing them to escape the trap. If the field is zero the m_F state is undefined, and the atoms can project themselves into an untrappable state when they move back into the field. To remedy this a constant magnetic field can be applied so that the minimum is no longer at $B = 0$ [30]. Atoms will still be confined, but a non-zero field will allow Zeeman level separation.

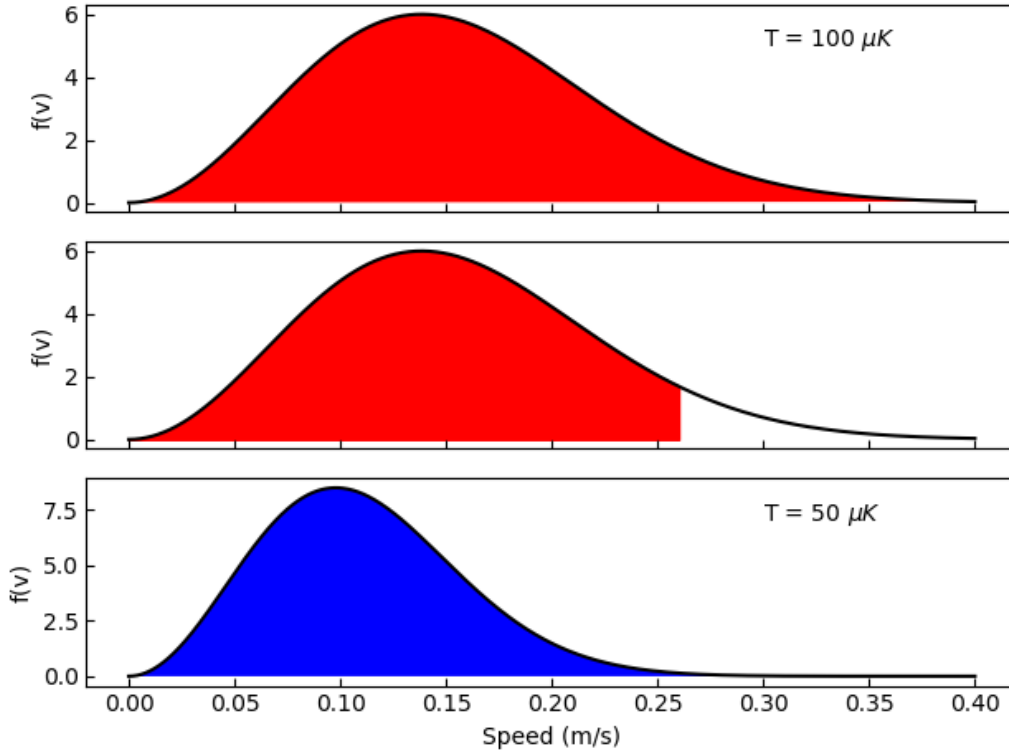


Figure 2.6: Plots showing the concept of evaporative cooling. Top: the atoms follow a Maxwell-Boltzmann distribution at $100 \mu K$. Center: Lowering the trap potential allows the “hot” atoms at the tail of the distribution to escape. Bottom: The atom re-thermalize at a lower temperature, $50 \mu K$.

2.6 Evaporative Cooling

In evaporative cooling the “hot” atoms in the large-velocity tail of the Maxwell-Boltzmann distribution are selectively removed from the trap, as shown in figure 2.6. Next, the atoms are allowed to re-thermalize, resulting in a new thermal distribution peaked at a lower temperature. The thermalization process takes 2.7 inelastic collisions on average [37]. This is similar to how steam carries off energy from a hot bowl of soup, allowing it to cool down. Evaporative cooling has allowed groups to cool atoms to nano-kelvin temperatures, and to make Bose-Einstein condensates.

Atoms can be evaporated out of a magnetic trap by using RF radiation to selectively remove hot, fast moving atoms. These atoms are found at the

edges of the trap, where the magnetic field, and thus the spacing between Zeeman levels, is high. By choosing a RF frequency resonant with transitions at the edge of the trap, transitions can be induced in atoms at the tail of the thermal distribution with the largest velocities, causing them to transition to untrappable states [38]. These hot atoms then leave the trap, allowing it to thermalize to a lower temperature. The RF radiation can then be swept to a lower frequency to evaporate atoms from the tail of the new distribution.

Another method for evaporative cooling is to lower the depth of an optical dipole trap by reducing the power of the beam, allowing hot atoms to escape [39].

2.7 Our Cooling/Trapping Procedure

We use cooling light which is red-detuned from the $F = 2 \rightarrow F' = 3$ transition on the ^{87}Rb D_2 line ($5S_{1/2} \rightarrow 5P_{3/2}$ transition). We choose this transition since the only dipole-allowed transition from the $F' = 3$ state is back to $F = 2$, which helps minimize the number of atoms that transition to another energy level, and out of the cooling cycle, through spontaneous emission. However, since the cooling light is detuned, there is still a possibility of off-resonant transitions, and some atoms could be excited via the $F = 2$ to $F' = 2$ transition. As a result, atoms could fall into the $F = 1$ state by spontaneous emission, bringing them out of the cooling cycle. To maximize the number of atoms available for cooling, we bring atoms that have fallen into the $F = 1$ state back on the cooling cycle by using repump light resonant with the $F = 1 \rightarrow F' = 2$ transition. A diagram showing the hyperfine structure of the ^{87}Rb D_2 line, with these transitions labeled, is shown in figure 2.7. The optical set-up for the repump light is described in section 2.7.1 and the set up for the cooling light is described in section 2.7.2.

Our first cooling step is a 2D MOT. Once atoms diffuse from the dispenser, a red-detuned push beam encourages them into the 2D-MOT region, where

they are cooled in two directions. This results in a “beam” of atoms directed towards the 3D-MOT region. A 3D MOT is used to trap the atoms. Once the trapping stage is complete, the 2D MOT and the magnetic field for the 3D MOT are turned off, allowing the captured atoms to be cooled via optical molasses. Next, the light is switched off, and the magnetic field is turned on, capturing the atoms in a magnetic trap. From here, evaporation cooling can be used to further cool the atoms if required. Finally, the magnetic field can be turned off, as an optical dipole trap is turned on and used to hold the atoms and transport them from the 3D-MOT chamber into the dilution fridge. If required, further evaporation cooling can also be done from the optical dipole trap. Implementation of this procedure is still in progress. The exact parameters, and final temperature of the atoms, will depend on many yet-to-be-determined factors, including the specific quantum devices being investigated.

2.7.1 Repump Optics

We use a MOGLABS CEL 780 nm external-cavity diode laser with a maximum output of 100 mW to generate the repump light. The optics for this set-up are shown in figure 2.9.

The total output from the laser is split into two beams using a half-wave plate and a polarizing beam splitter. A small portion is used for laser locking and frequency monitoring. The rest is used to sent to the vacuum system via fibres and used to pump atoms out of the $F = 1$ state.

The locking/monitoring light is further split 3 ways. A portion of the light is used for beat-note locking and monitoring with a wave-meter, some light is sent to a Fabry-Perot cavity for monitoring, and the remaining light is used for locking via saturated-absorption spectroscopy. The light used for saturated absorption is split into two beams: a strong pump beam and a weak probe beam. The pump beam is shifted by 160 MHz using a double pass through an acoustic-optical modulator (AOM). When the light passes through the AOM, it will receive a momentum kick from an acoustic wave, which, through con-

ervation of momentum, shifts the light’s frequency. This results in the laser being locked 80 MHz below resonance for the $F = 1 \rightarrow F' = 2$ transition. The use of the AOM allows the beam to be modulated using a signal generated by the MOGLABS laser controller, a requirement for the locking process. The probe beam passes directly through the cell and into a photodiode. The signal from the photodiode is sent to the MOGLABS laser controller, which performs small-signal detection in order to lock the laser.

Since the laser is locked 80 MHz below resonance, additional AOMs are used to shift the repump light frequency back on resonance. The repump light passes through an AOM, and the first diffraction order is shifted up 80 MHz, and is used for the 2D MOT repump light. The 0th order is sent through another AOM to be shifted back to resonance for use as 3D repump light. Using separate AOMs for the 2D and 3D repump light allows us more control over the frequency, as well as control over the power in each beam.

2.7.2 Cooling Optics

For the cooling light we use a MOGLABS MSA 780 nm laser. This laser has two outputs, one from the seed beam (22 mW) and one after the beam has passed through the tapered amplifier (2 W). It is locked using beat-note locking.

The seed beam is used to lock the laser and monitor frequency. It is split into two beams. One is used for beat-note locking, and the other is sent to a Fabry-Perot cavity for frequency monitoring. Half-wave plates and beam splitters are used to divide the light, and control the power in each beam. The unused light is dumped into a beam-block.

The light from the amplified beam is split multiple times, allowing individual control over the frequency and power in each beam. The first path is the “2D-MOT” path. Some of this light is split off and shifted by -96 MHz to be resonant with the $F = 2$ to $F' = 2$ transition for optical pumping. The

remaining light is sent through an AOM double pass. After the double pass, the light in the first-order beam is shifted by 2×80 MHz. This light is used as cooling light in the 2D MOT. The 0th-order beam is shifted 80 MHz from the first pass through the AOM. It is sent through another AOM and is shifted by 99 MHz to be resonant with the $F = 2$ to $F' = 3$ transition for imaging.

The second path is the “3D-MOT” path. This light is sent through an AOM double pass, similar to what was done on the 2D-MOT path. The first order beam from the double pass is shifted by 2×80 MHz, and is red-detuned from the $F = 2$ to $F' = 3$ transition. This light is used as cooling light in the 3D MOT. Before the fibre couple for the 3D-MOT cooling light there is a waveplate and beam splitter. This will allow more control over the beam power, and offers the possibility to create another beam path if needed. The light found in the 0th-order after the double pass is shifted by 80 MHz. It goes through another AOM, receiving a 103 MHz shift. This light is used in the push beam.

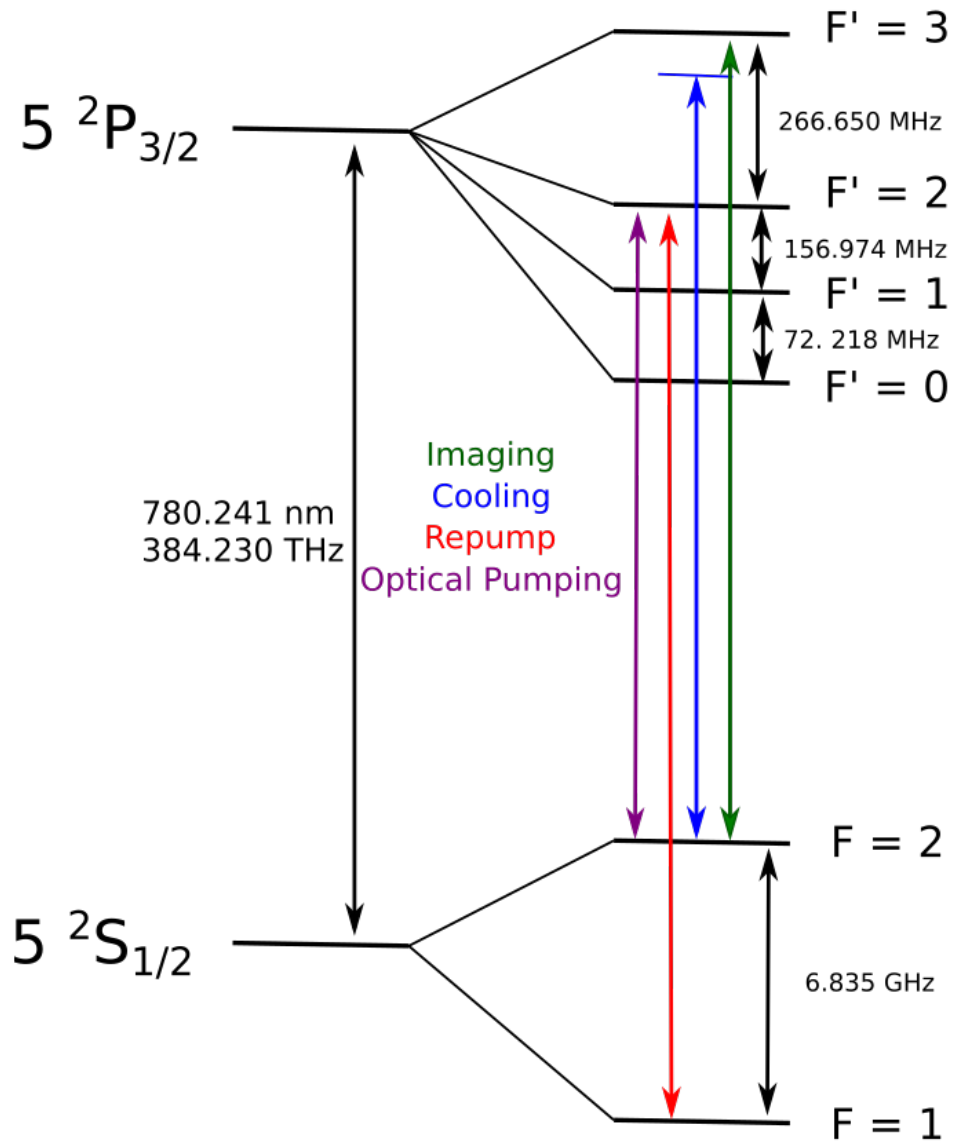


Figure 2.7: Diagram showing the hyperfine structure on the ^{87}Rb D_2 line. The transitions that we use for cooling, imaging, repump, and optical pumping are marked on the diagram. Adapted from [32]

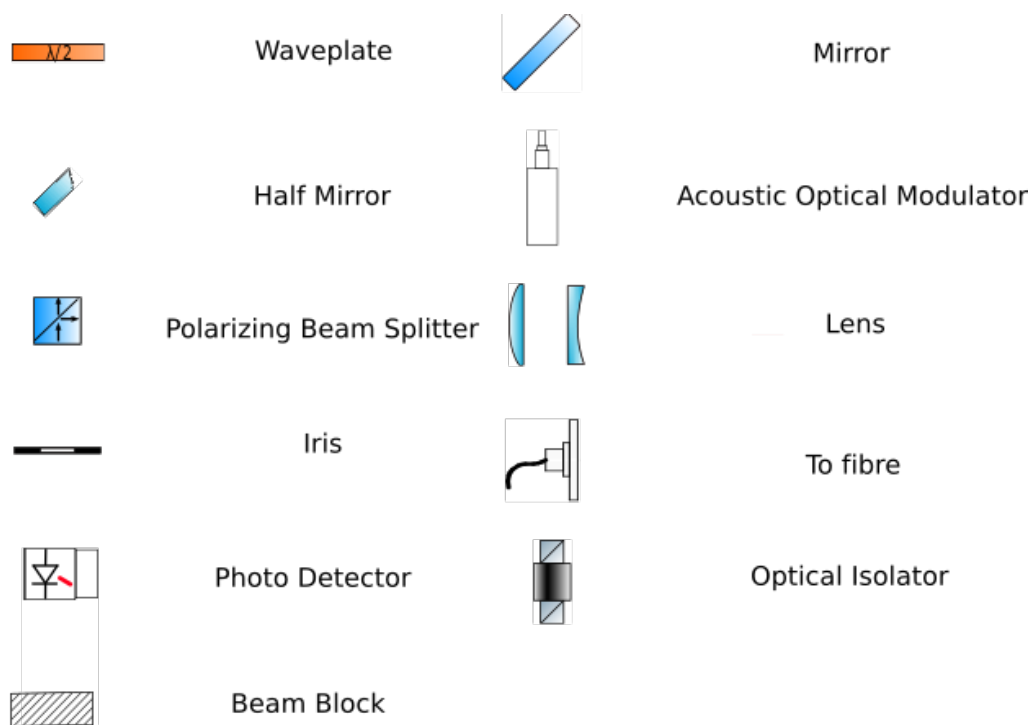


Figure 2.8: Legend showing all of the components used in our optical set-ups.

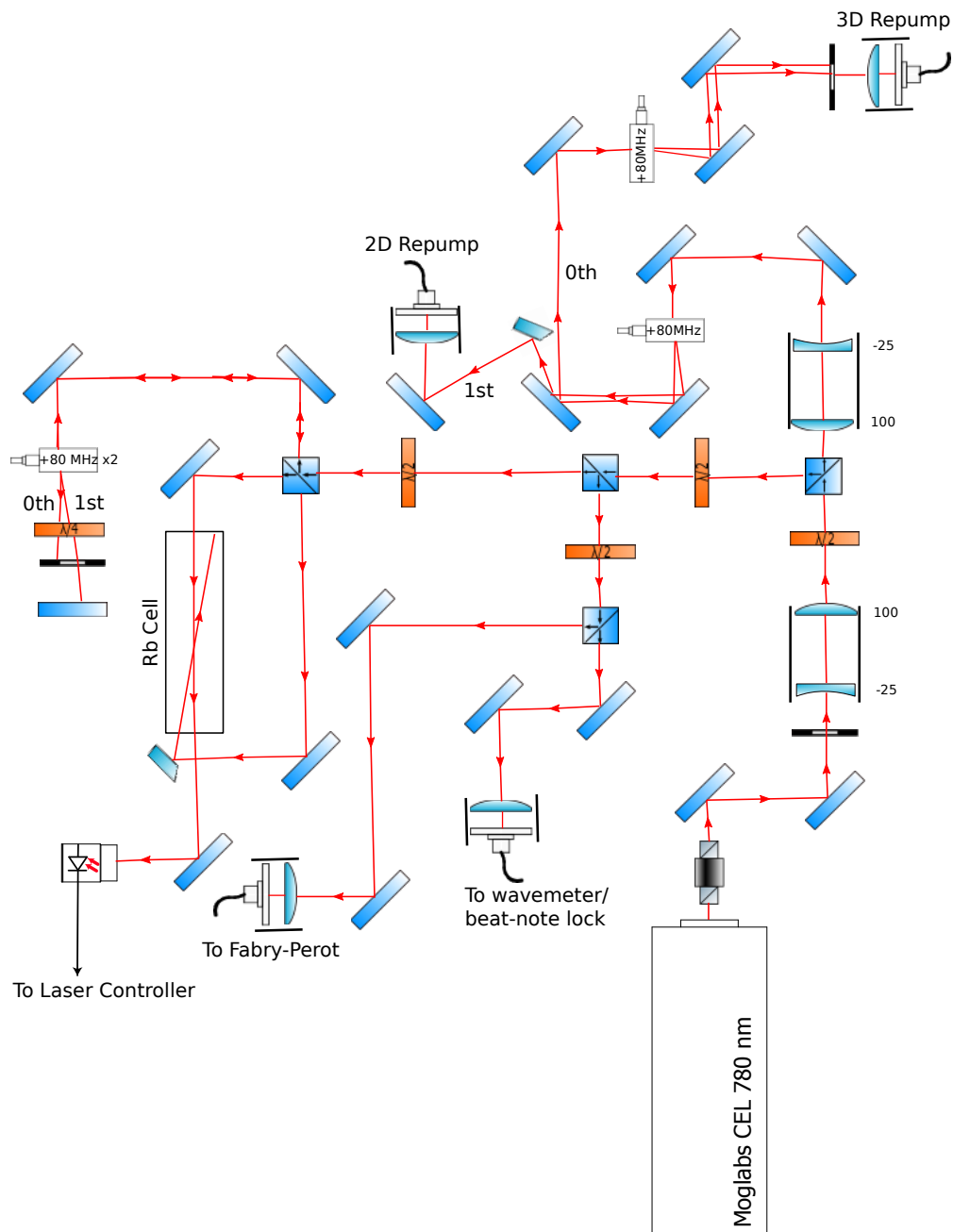


Figure 2.9: The optics set-up for the repump light. A legend for the components can be found in figure 2.8

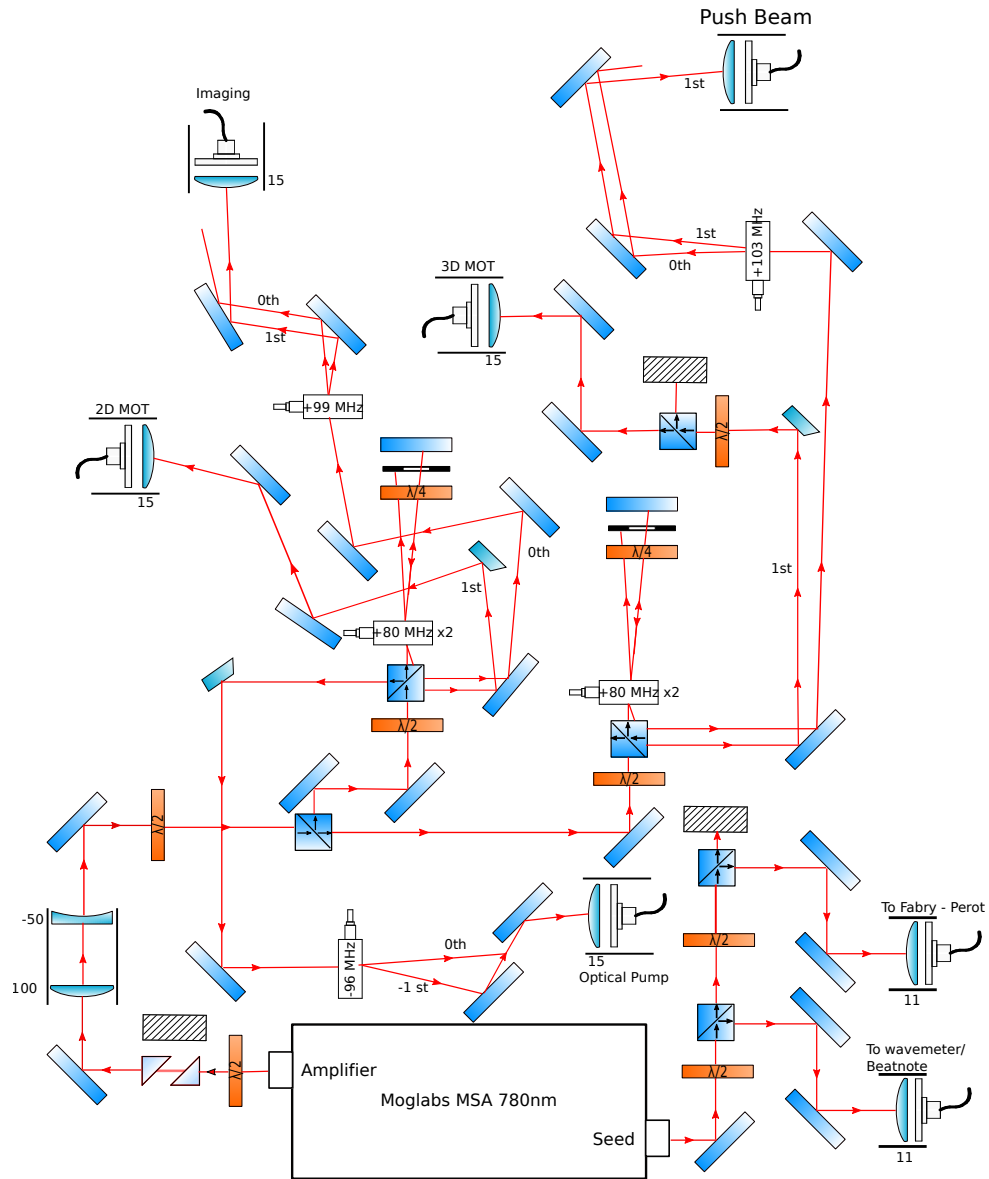


Figure 2.10: The optics set-up for the cooling light. A legend for the components can be found in figure 2.8

Chapter 3

Apparatus

The proposed hybrid quantum system requires a new apparatus which combines a dilution refrigerator and an ultra-high vacuum chamber where the atoms are laser cooled. A CAD drawing of the apparatus is shown in figure 3.1. This chapter details the design of this apparatus, and the construction of the cold atoms portion of the new apparatus.

3.1 Design

We have designed a custom vacuum chamber where the atom cooling portion of the experiment will take place. This system is capable of achieving ultra-high vacuum (UHV) in order to minimize background pressure. Any background molecules or atoms could collide with the ^{87}Rb that we are studying, causing heating, or causing atoms to escape during trapping phases. Where possible, we have used non-magnetic parts made of 316-stainless steel to avoid stray magnetic fields interfering with the cooling and trapping processes.

The system has three main parts: I. the dispenser region, II. the 2D-MOT region, and III. the 3D-MOT region. Each of these is described below. A 3D model of the system is shown in figure 3.2.

3.1.1 Dispenser Region

The dispenser region is labeled I in figure 3.2. In this region, we connect multiple components to the system via a 6-way cross. Optics for the push

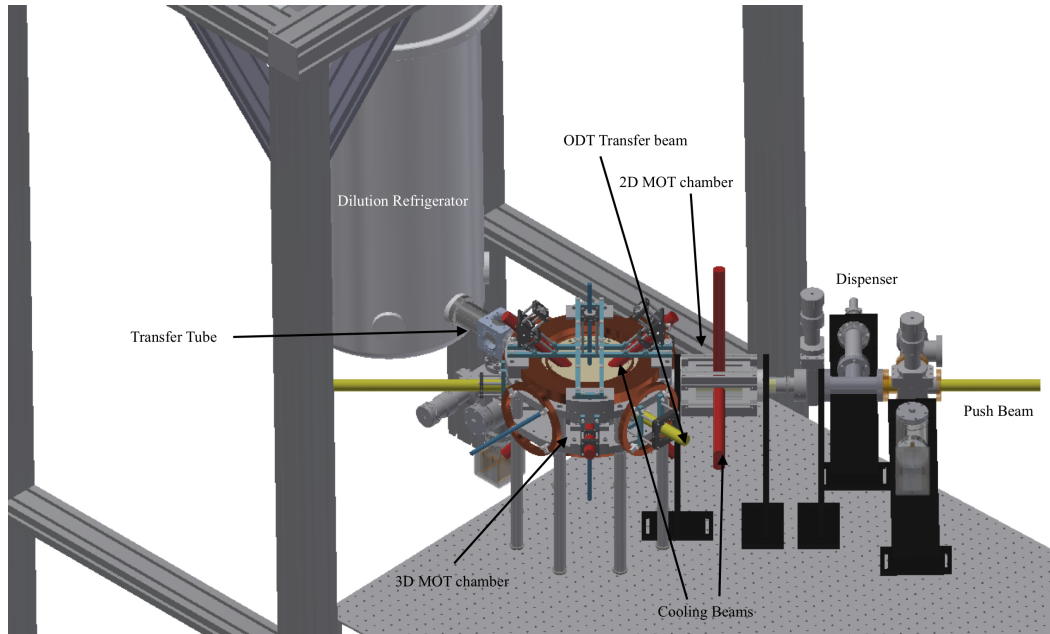
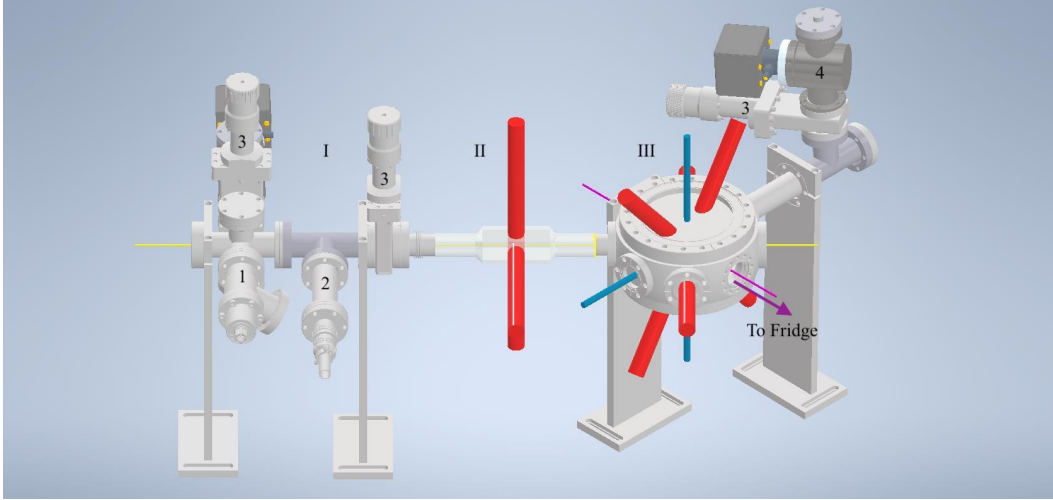


Figure 3.1: CAD drawing of the new apparatus showing the cold-atoms vacuum chamber and the dilution fridge. Image courtesy of Myles Ruether.

beam are mounted to the furthest end, and directed straight along the axis into the 2D-MOT chamber. The push beam is shown in yellow in Figure 3.2. Also connected to this cross is a valve for the turbo pump, part number 54132-GE02 from Kurt J. Lesker, labeled 1 in figure 3.2. The turbo pump will be used to remove air from the chamber in the first stage of vacuum, before the ions pumps are activated to get to UHV. Opposite to the valve is a custom-made tee which houses an ion pump and a non-evaporable getter (NEG). The ion pump/ NEG combination is labeled 4 in figure 3.2. We have placed a gate valve, part number 302001 from MDC, between the ion pump/NEG tee so that it can be kept under vacuum if we open the rest of the system. All gate valves are labeled with the number 3 in figure 3.2. After the 6-way cross, we have inserted a tee. The tee allows us to attach the Rb dispensers, which are soldered to wires inside a 4-pin electrical feed-through, part 9142004 from MDC. After the dispenser and before the 2D MOT we have used another gate valve to separate this region from the rest of the system, allowing us to change the dispensers without requiring a full bake.

(a)



(b)

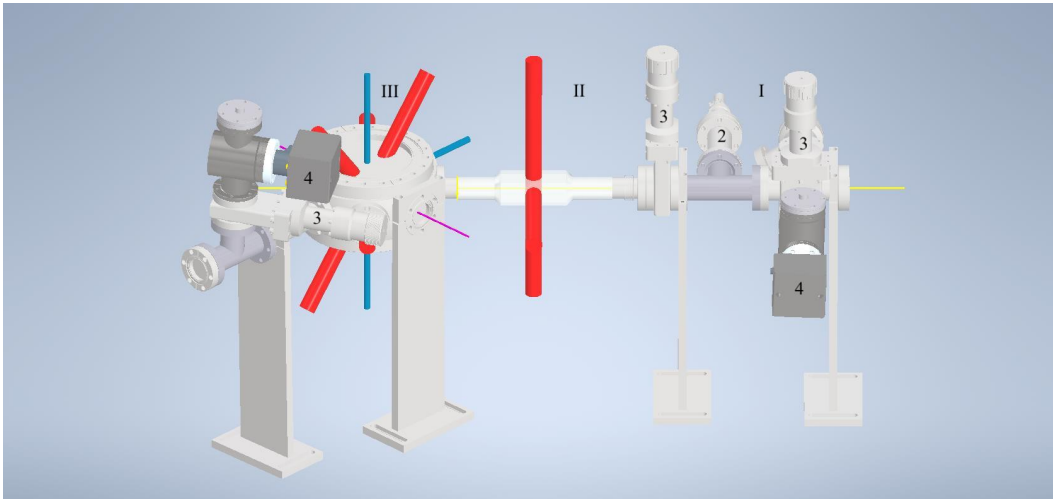


Figure 3.2: 3D model of the UHV system. The labelling system is as follows: I Dispenser region, II 2D-MOT region, III 3D-MOT region. 1. Valve for turbo pump, 2. Dispensers, 3. Gate valves, 4. Ion pumps. Beams are color coded, yellow is push beam, red is MOT beam, blue is imaging, and purple is the transport ODT beam. a) View from front side, b) View from back side. The system is shown without any optics or coils mounted for clarity.

3.1.2 2D-MOT Region

The 2D-MOT region is labeled II in figure 3.2. We use a custom-made glass cell from Precision Glass Blowing for the 2D MOT. The main part is a rectangular glass cell that is 100 mm long, 40 mm high, and 40 mm wide. The large glass surface provides optical access for two sets of counter-propagating laser beams. This glass cell has been welded onto 2-3/4"-conflat flanges on both ends to allow it to be secured to the other conflat components. The end attached to the dispenser cross has a bellows connected to the flange.

To create the magnetic fields necessary for the MOT, two coils are mounted around the cell. They are made of awg 12 copper wire with 2.2 mm diameter and have 25 turns each. The coils are mounted in supports which were machined in house. The supports are hollow in the region where the coils are attached to allow for water cooling as the coils will heat up when we run current through them. The supports were designed so that standard ThorLabs rails could be screwed in to mount optics.

Repump and cooling light is carried by fibres from the optics table. Once the light exits the fibre it is focused with two cylindrical lenses, focal lengths 75 mm and 100 mm.

Differential Pumping Tube

To pass from the 2D MOT to the 3D MOT, atoms go through a differential-pumping tube. We used a 6" long piece of 316-stainless steel tubing with an outer diameter of 3/8" and wall thickness of 0.035". This extends from the end of the 2D-MOT cell into the 3D-MOT chamber.

When the atoms leave the 2D-MOT region they have been slowed in two directions, resulting in a beam of atoms with velocity along one direction. Atoms that were not sufficiently cooled in the directions transverse to their

propagation will diffuse out of the region before they enter the tube, meaning that “hot” atoms will not make it into the larger chamber.

3.1.3 3D-MOT Region

After the differential pumping tube, the atoms enter a large 3D-MOT chamber, where the remaining cooling steps are carried out. This chamber is an 8-inch spherical octagon from Kimball physics made from 316-stainless steel. The circumference of the chamber is equipped with 8 2-3/4-inch CF flanges, and there are 8-inch CF flanges on the top and bottom.

The atoms will enter the chamber from the 2D-MOT cell through one of the smaller openings on the circumference of the chamber. Directly opposite this, a viewport allows the push beam to exit the chamber without any back reflection. We also have 3 pairs of mutually orthogonal 3D-MOT beams (red beams in figure 3.2) directed into the chamber. Two sets are entering through the large top/bottom viewports and are angled at -45 and 45 degrees with respect to vertical, respectively. The third beam pair is in the horizontal plane, entering through the viewports on the circumference of the chamber. Similar to the 2D MOT, light for the 3D MOT is brought to the chamber from the optics table via fibres, and combined with the repump light. Taras Hrushevskyi designed custom mounts to attach optics to the 3D-MOT chamber. A model of the apparatus with the optics and coils mounted is shown in figure 3.3. The light from the fibre is focused to create one inch beams.

The optical dipole trap is shown in purple in figure 3.2. The optics for this beam are mounted on the viewport between the exit to the 2D MOT and the 3D-MOT beam. The flange directly opposite will be connected to a tube leading to the fridge, allowing for optical transport of the atoms.

Imaging is done along two perpendicular axes: one horizontal and one vertical. The imaging beams are shown in blue in figure 3.2. We will use resonant absorption imaging to determine the cloud density and temperature.

The imaging beam on the horizontal axis passes through a tee. This allows a gate valve, an ion pump, and non-evaporative getter (NEG) to be mounted on the top end of the tee, while also giving the imaging beam an obstruction-free path out of the chamber.

All of the viewports are fused silica and made from non-magnetic 316-stainless steel. We get them from the company MPF.

3D-MOT coils

A large set of coils are used to create the magnetic field gradient required for the 3D MOT. They were designed to go around the viewports so as not to restrict optical access. These coils are made out of hollow, square copper wires. The wire cross section is 5.5 mm. The hollow core allows cool water to run through the coils, preventing heating caused by the high currents required to create the necessary magnetic field gradients. The coils are separated by 75 mm and have an inner radius of 105 mm. Each coil is 9 turns wide and 7 turns tall. They are capable of producing an axial gradient of $0.42719 \frac{G}{cm \cdot A}$ (170 G/cm at 400 A) and a radial gradient of $0.20043 \frac{G}{cm \cdot A}$. The coils are mounted to the chamber using custom mounts designed by Taras Hrushevskiy and are shown in figure 3.3.

Bias Coils

Stray magnetic fields may cause the MOT centre to shift away from the centre of the chamber, where all of the cooling, trapping, and imaging beams overlap. In order to compensate for this, three set of Helmholtz coils are used to create a bias magnetic field, which can be adjusted throughout the experiment. These coils are made out of awg 12 copper wire, with a 2.2 mm diameter circular cross section. The size of each coil, along with the magnetic field that they produce, is given in table 3.1. We are able to run upto 20 A of current through each coil.

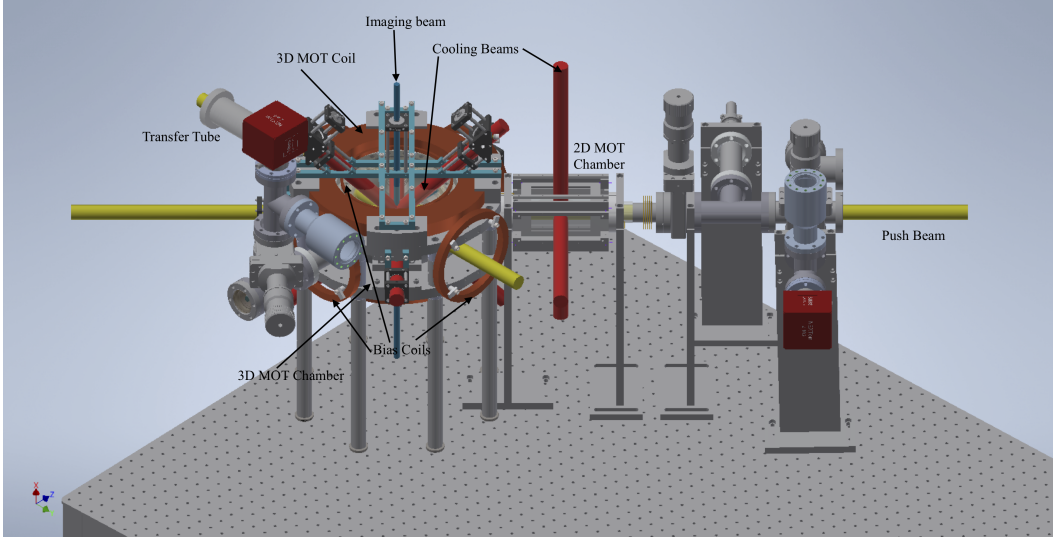


Figure 3.3: CAD drawing of the vacuum system with coil and optics mounts. Image courtesy of Taras Hrushevskiy.

Axis	Number of Turns	Separation (mm)	Radius (mm)	Field (G/A)
X	36	350	70	0.33
Y	36	350	70	0.33
Z	6	115	77	0.5

Table 3.1: The dimensions of each set of bias coils, along with the magnetic field that they produce.

3.2 Cleaning, assembly, and bakeout

When the vacuum parts arrive, it is possible that there is some residue remaining on them from the manufacturing process. This residue will off-gas, prolonging the baking process, or making it impossible to reach ultra-high vacuum. To prevent this from happening each component is cleaned before assembling the vacuum chamber. We start by washing them with Alconox Alcojet[®] low-foaming powered detergent and warm tap water. Then, we rinse each part with tap water, followed by distilled water. Finally we use two solvents, acetone followed by methanol, to remove any remaining residue. All parts are cleaned following this procedure, except for the pumps, valves, and the 2D-MOT cell. Additionally, to prevent any of the oil from our skin, which is difficult to remove through baking and pumping, from contaminating the parts, we wore nitrile gloves whenever we handle the parts.

After cleaning, we assembled the vacuum system. A silver-plated copper gasket was placed between each part. The knife edges on the conflat flanges cut into these gaskets, forming a tight seal. The silver plating prevents the parts from fusing together at the high temperatures required for the bake. We used silver-plated bolts, again to prevent the parts from fusing during bake out, in order to assemble the parts. When tightening the bolts each both is tightened by a small amount, about an eighth of a turn, before moving to the next bolt. Moving in small steps will apply even pressure to the gasket, preventing it from being pushed out of place. This process is repeated in a circle until the desired torque is reached. The 2- 3/4-inch flanges are tightened to 144 inch-pounds, and the 8-inch flanges are tightened to 180 inch-pounds, as per the specification given on Kurt J. Lesker's website [40]. A torque wrench was used whenever possible, however some parts fit together closely thus requiring the use of a smaller wrench. In this case we did our best to "feel" for the correct torque and to ensure a similar torque for each bolt.

After the system was assembled, it needs to be baked in order to release

organic contaminants. The first step in this process was to wrap heater tapes around each part. To avoid damaging the glass on the 2D-MOT cell we surrounded it with a metal frame, and wrapped the heating tapes around the frame. Then we attached thermocouples in order to monitor the temperature. Our system has both glass and metal parts, which have different thermal conductance rates. In order to ensure even heating, and to avoid damaging any of the glass/metal joins we placed two thermocouples on parts made of both materials; one on the glass portion, and one on the metal portion. Finally, we wrapped the entire system in tinfoil to help keep the heat in and to ensure even heating of the system.

The system has been prepared for the bake, but due to a lab closure we have been unable to complete the baking process.

Chapter 4

Atom Transport

In our apparatus, cold atoms are prepared in a vacuum system outside of the dilution fridge. To couple the atoms to the cryogenically-cooled devices inside the fridge we will need to transport the atoms from the centre of the 3D-MOT chamber to the edge of the dilution fridge. This distance is about 60 cm.

Multiple groups have demonstrated atom transport using a variety of methods including a moving optical lattice [41], a magnetic conveyor belt consisting of a series of magnetic coils used to move the center of a magnetic trap [25,42], optical tweezers which use a focusing lens mounted on a translation stage to move an optical dipole trap [24,43], and a moving optical dipole trap created using a focus tunable lens [44], [45].

We choose to use a focus tunable lens to create a moving optical dipole trap based off of the work of the Esslinger group at ETH Zurich [44,45]. This set up is compact, does not require the winding of numerous magnetic coils, and minimizes vibrations caused by moving parts. Below I will explain the theory behind this set up, show some calculations of trap depth and scattering time, and discuss simulation results.

4.0.1 Theory: Moving ODT

We choose to transport the atoms using a moving ODT. Atoms in an ODT are confined at the focus of a Gaussian beam, as described in section 2.4. If

the focus point moves, the atoms, still confined, will move with it. An easy way to accomplish this is to change the focal length of the focusing lens. The company Optotune manufactures focus tunable lenses. These lenses have a fluid-filled membrane surrounded by a coil. By running current through the coil a force can be exerted on the lens, changing its shape, and thus its focal length. Changing the current in the lens would then equate to moving the atoms. However, when the focal length of the lens is changed the size of the waist-at-focus will also change, which is undesirable as it will change the trap depth and frequency, which will heat atoms and cause them to be lost out of the trap. Thankfully there are set-ups which allow the waist size to be kept constant throughout the trap motion [44, 45]. We were originally inspired by a 2014 paper [44], and after conversing with the authors decided to adapt an updated version of their set-up [45] for our experiment.

The set-up is as follows: first, the laser beam is collimated by a telescope consisting of two spherical (non tunable) lens. The focal length of the lenses used in the telescope determines the incoming beam size, which sets the size of the focus waist.

Next, the collimated beam goes through the focus tunable lens. We use Opotune model EL-16-40-TC. This model has the largest aperture of the available models, 16 mm. The glass casing for our lens is anti-reflection coated for 1064 nm, the wavelength of the laser used for our ODT. The lens operates with both positive and negative currents, allowing diverging and converging operation. A final spherical lens (non tunable) with focal length f_3 is placed a distance f_3 in front of the tunable lens. It can be shown [45] using ray propagation matrices for Gaussian optics that if this condition is satisfied, the divergence angle of the beam after it passes through the final lens is $\alpha = \frac{r_0}{f_3}$, where r_0 is the radius of the beam when it hits the tunable lens, which is constant regardless of focal length of the tunable lens. A constant divergence angle means a constant focus waist and trap depth.

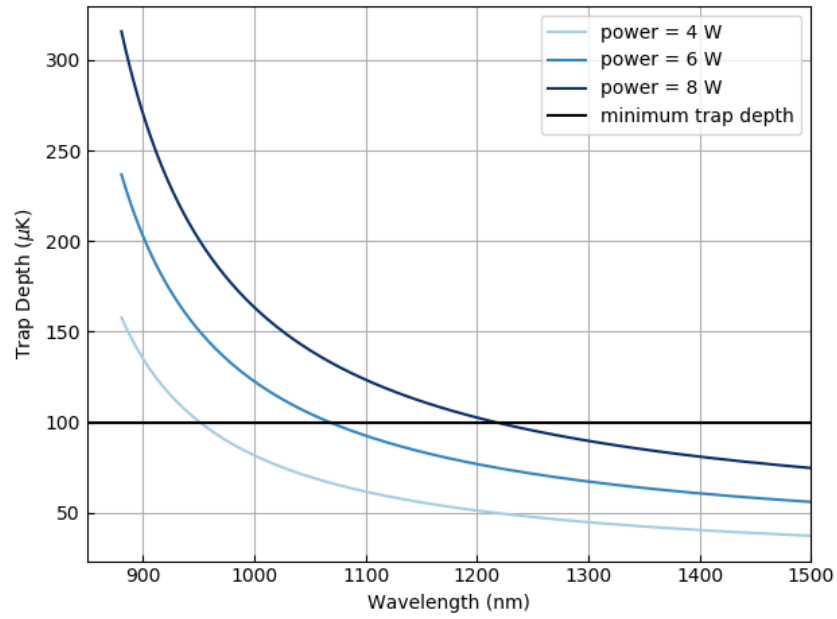
4.1 Results

4.1.1 Calculations

As can be seen in equations (2.33) and (2.34) the scattering decreases much faster as a function of detuning than the potential. This is shown in figure 4.1. In order to reduce the number of scattering events, which would result in heating, we choose to use a 1064 nm laser, which is far detuned from the 780 nm resonant transition in ^{87}Rb . To contain the atoms, the trap depth must be about 3 times the temperature of the cloud. We anticipate cooling the atoms to about $30 \mu\text{K}$, and will require that the trap have a minimum depth of $100 \mu\text{K}$. Our laser has a maximum output of 10 W. Due to losses in the optical isolator and from reflections we anticipate only having around 6 W of power available for trapping. If the beam has a waist at focus of $70 \mu\text{m}$ ($140 \mu\text{m}$ diameter) we will achieve this trap depth.

Before we start the transport process, it is important to check that it is possible to focus the beam to a waist of $70 \mu\text{m}$ and move it 60 cm. I have written code in python that uses the ABCD matrices to trace the beam's size at specified distances from the final lens. If the collimated beam waist is 2.5 mm and we use a focusing lens with $f_3 = 500 \text{ mm}$ after the tunable lens, the beam waist will be $67 \mu\text{m}$, very close to the desired waist of $70 \mu\text{m}$. The optical power (inverse of focal length) of Oportune lens model EL-16-40-TC that we are using ranges from -2 m^{-1} to 3 m^{-1} . As shown in figure 4.2, if the optical power starts at 0.65 m^{-1} the the focus is initially 340 mm away from the final lens. The spherical octagon where the atoms are cooled has a diameter of about 200 mm, it is therefore possible to have the focus of the beam at the center of the chamber with appropriate optics placement. If the optical power is decreased to -1.57 m^{-1} the focus will be located 940 mm away from the lens, or 60 cm from the starting position. Transport over the desired distance is feasible with a focus tunable lens.

(a)



(b)

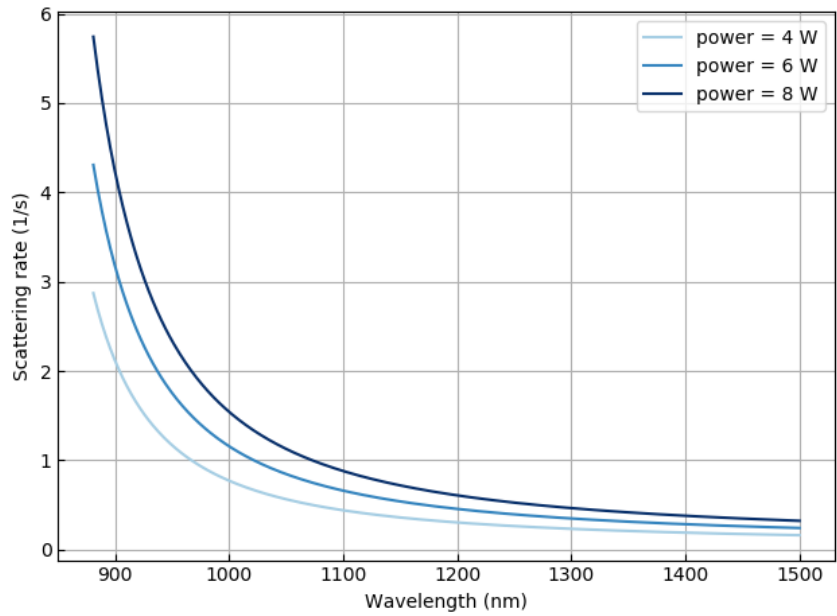
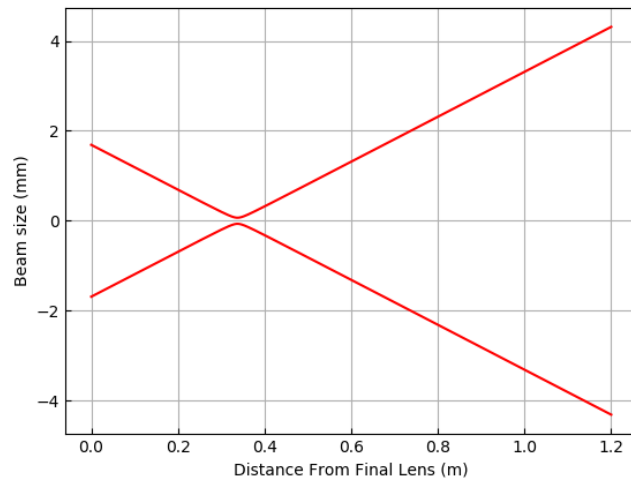


Figure 4.1: (a) Depth of an optical dipole trap with beam radius of $70 \mu\text{m}$ as a function of trapping wavelength, at laser powers of 4, 6, and 8 W. We require a minimum depth of $100 \mu\text{K}$, which is shown in the plot. (b) Scattering in an optical dipole trap with beam radius of $70 \mu\text{m}$ as a function of trapping wavelength, at laser powers of 4, 6, and 8 W.

(a)



(b)

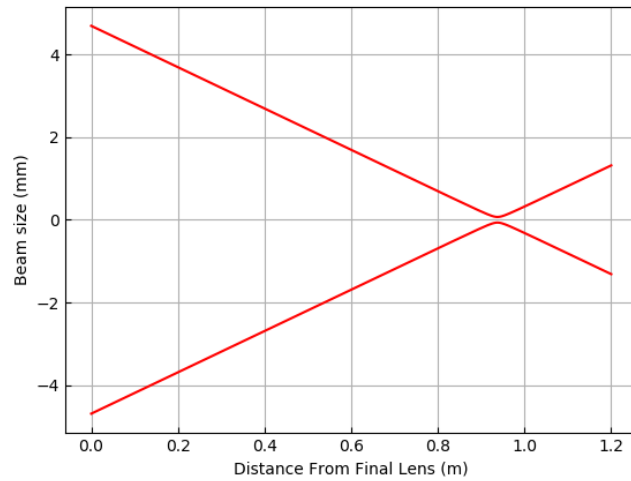


Figure 4.2: Figure showing the size of the transport beam after the focusing lens. (a) The focus tunable lens is set to optical power 0.65 m^{-1} . (b) The focus tunable lens is set to optical power -1.75 m^{-1} .

4.1.2 Temperature Control

It has been previously observed that due to temperature fluctuations, the focal length of the tunable lens is unstable [45]. Although the lens comes with a driver that should adjust focal length to compensate for temperature changes, our application requires finer control over focal length than this device offers. To mitigate this, a temperature controller is needed. This controller will measure the lens temperature using the sensor built into the lens. Based off of the factory calibrated data read from the lens' memory, the temperature controller will calculate the necessary adjustment to the current in the lens in order to give the specified focal length. James Chaulk is currently building a temperature controller.

4.1.3 Simulations

Due to a lab closure, we were unable to cool the atoms, and did not reach a point where we were able to test the transport system, so I did a simulation of the transport process. The goal was to determine a transport path shape, and the time it would take to transport the atoms. Ideally, to avoid increasing the temperature of the cloud, or losing atoms during the transport process the transport would be adiabatic, and take place over a time much greater than the oscillation period in the trap. The transport will take place along the z-axis. We approximate the optical dipole trap as a harmonic oscillator, and the potential is given by equation (2.37). The frequency of oscillation along the z-axis is given by

$$\omega_z = \sqrt{\frac{2U_0}{mz_R^2}}. \quad (4.1)$$

In our case, $U_0/k_B = 100 \mu K$, m is the mass of an ^{87}Rb atom, and z_R is the Rayleigh range, given by

$$z_R = \frac{\pi w_0^2}{\lambda}, \quad (4.2)$$

where w_0 is the beam waist, and λ is the wavelength of the trapping light. For our set up, $\omega_z \approx 2\pi \cdot 1.12 \text{ Hz}$. This gives a period of $T = 0.89 \text{ s}$. To ensure adi-

abaticity, the transport will need to occur over a time $t > 1000T \approx 15$ min. Our measurements use a destructive imaging method, and require that the atoms be replaced frequently. We are unable to wait almost 15 minutes between each iteration, therefore we must find a way to transport the atoms more rapidly.

It is possible to transport atoms within a shorter time frame, as shown by Couvert *et al* [46]. Their theoretical result shows that the absolute value of Fourier transform of the optical dipole trap's velocity profile gives the change in amplitude of atom cloud's oscillations [46]. This agrees well with experiment. Up to a scale factor, the experimental change in amplitude follow the same profile as the Fourier transform. Although there was some additional heating due to equipment instability, when the Fourier transform is zero there are no residual oscillations, and thus the no heating contribution due to the motion of the cloud [46].

We decided to take a different approach to modeling this problem. Each atom will have an equation of motion, which can be derived from the Lagrange equation:

$$\frac{\partial L}{\partial q} - \frac{d}{dt} \left(\frac{\partial L}{\partial \dot{q}} \right), \quad (4.3)$$

where q is a coordinate, and L is the Lagrangian given by:

$$L = T - U, \quad (4.4)$$

where T is the kinetic energy, and U is the potential energy. To account for the trap's motion along the z -direction, we add an additional potential term, $ma_t(t)z$, where $a_t(t)$ is the trap acceleration, to equation (2.37). Our Lagrangian is then

$$L = \frac{1}{2}m\dot{\mathbf{r}}^2 + \frac{1}{2}m\mathbf{r}^2\dot{\theta}^2 + \frac{1}{2}m\dot{\mathbf{z}}^2 + U_0 - \frac{1}{2}m\omega_r^2\mathbf{r}^2 - \frac{1}{2}m\omega_z^2\mathbf{z}^2 - ma_t(t)\mathbf{z}. \quad (4.5)$$

We can use equation (4.5) in equation (4.3) to find the equations of motion in the frame of the moving optical dipole trap:

$$m\ddot{\mathbf{r}} = m\mathbf{r}\dot{\theta}^2 - m\omega_r^2\mathbf{r}, \quad (4.6)$$

$$m\ddot{\theta}\mathbf{r}^2 = -2m\mathbf{r}\dot{r}\dot{\theta}, \quad (4.7)$$

$$m\ddot{\mathbf{z}} = -m\omega_z^2\mathbf{z} + ma_t(t). \quad (4.8)$$

Since the trap only moves in the z -direction, and the equation of motion for z is independent of r and θ , we choose to only look at the z -component of motion in the simulation.

The next step is to describe the initial cloud of cold atoms. The Boltzmann factor gives the density of the cloud [36]:

$$n = n_0 e^{\frac{-U(r)}{k_B T}}. \quad (4.9)$$

Using a harmonic potential in the z -coordinate gives, with appropriate normalization,

$$n(z) = \sqrt{\frac{m\omega_z^2}{\pi k_B T}} e^{-m\omega_z^2 z^2 / k_B T}, \quad (4.10)$$

which is a normal distribution with mean zero, and standard deviation $\sqrt{\frac{k_B T}{m\omega_z^2}}$. Python provides built in functions to generate a sample from a normal distribution, and the histogram of positions can be fit to extract the temperature. Momentum also follows a normal distribution:

$$\sqrt{\frac{1}{2\pi m k_B T}} e^{-p_z^2 / 2m k_B T}. \quad (4.11)$$

The initial distribution of positions and momentum is given in figure 4.3.

I have written python code which integrates the equations of motion for each atom in the distribution. At each time step it fits the position distribution to equation (4.10) and extracts the position and temperature. After the trap has finished moving, the atoms are allowed to sit for a period of time in the stationary trap, where the atoms oscillate about the center of the trap with frequency ω_z . The temperature extracted from the fit remains relatively constant throughout the process as the equations of motion do not take interactions between atoms into account. However, the oscillations represent an increase in potential energy, $\frac{1}{2}m\omega_z^2 z^2$, which would result in an increase in temperature when the atoms re-thermalize through collisions. This temperature change can be estimated by equating thermal and potential energy:

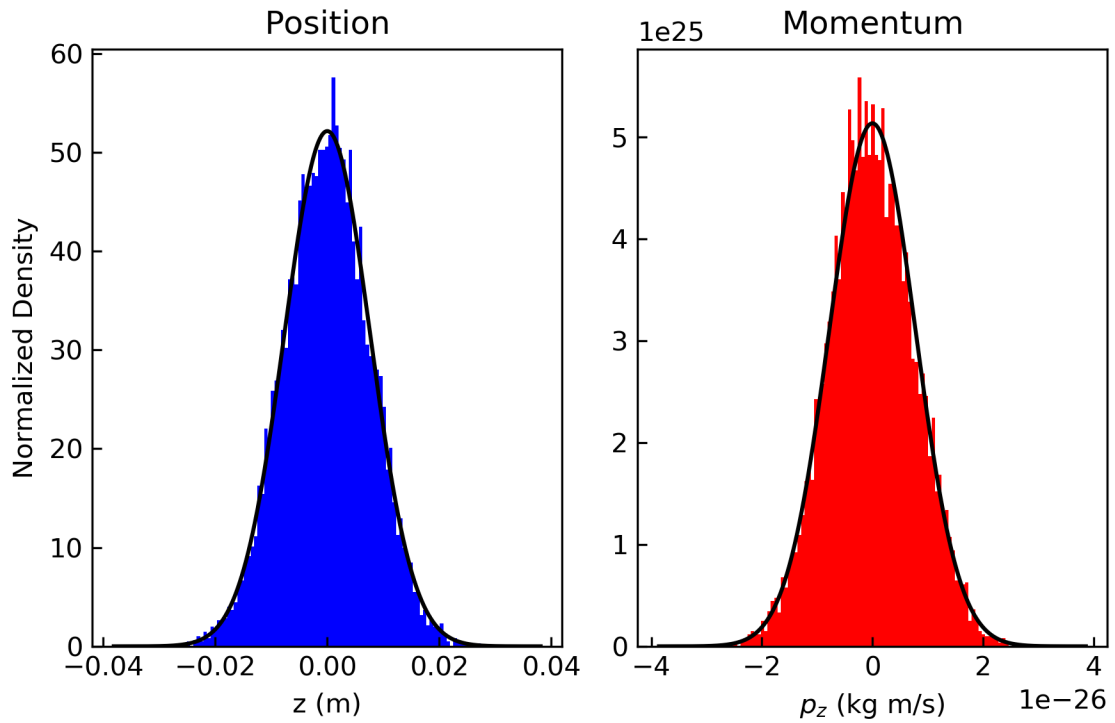


Figure 4.3: The initial distribution of atom position and momentum in the z -coordinate, generated from equations (4.10) and (4.11). The histograms show the position (left) and momentum (right) values, and the black lines shows the normal distribution fit to the distribution. The temperature extracted from the fit to position (momentum) is $30.2 \pm 0.5 \mu K$ ($30.4 \pm 0.6 \mu K$).

$$\frac{1}{2}k_B\Delta T = \frac{1}{2}m\omega_z^2\langle\Delta z^2\rangle, \quad (4.12)$$

$$\Delta T = \frac{m\omega_z^2\langle\Delta z^2\rangle}{k_B}. \quad (4.13)$$

The oscillations following the transport period are fit to a sine wave,

$$A\sin(Bt + C) + D. \quad (4.14)$$

The amplitude, A , of the oscillations can be determined from the fit and used to find the temperature increase:

$$\Delta T = \frac{m\omega_z^2\langle A^2\sin^2(\omega_z t)\rangle}{k_B} = \frac{m\omega_z^2 A^2}{2k_B}. \quad (4.15)$$

We expect the lifetime of atoms in the trap to be around 30 seconds. Ideally we don't want to wait for the atoms to arrive between measurements, so transports times less than the trap lifetime are desirable. We have set a maximum wait time of ten seconds, however, the shorter the better. We also need the amount of heating to be less than the trap depth (100 μk). The atoms should come to a stop at the final position, which imposes the conditions $z_c(0) = 0$, $z_c(t_f) = d$, $\dot{z}_c(0) = 0$, and $\ddot{z}_c(t_f) = 0$. We have investigated 3 different velocity profiles that meet these conditions in order to find the best option for our set up.

Gaussian Velocity Profile

When the velocity profile is Gaussian, the trap trajectory will be in the shape of an error function. Position, velocity, and acceleration are shown in figure 4.4 and are described by the following equations:

$$z_c(t) = \frac{|F_f - F_i|}{2} \left[\operatorname{erf}\left(\frac{6t}{t_f}\right) + 1 \right] + F_i, \quad (4.16)$$

$$\dot{z}_c(t) = \frac{6}{\sqrt{\pi}} \frac{|F_f - F_i|}{t_f} e^{-9(2t/t_f)^2}, \quad (4.17)$$

$$\ddot{z}_c(t) = \frac{6}{\sqrt{\pi}} \frac{|F_f - F_i|}{t_f} e^{-9(2t/t_f)^2} \left(\frac{-72t}{t_f^2} \right), \quad (4.18)$$

where t_f is the transport duration, F_f is the final trap position, in this case 60 cm, and F_i is the initial trap position, in this case 0 cm. Plots of the position, velocity, and acceleration are shown in figure 4.4.

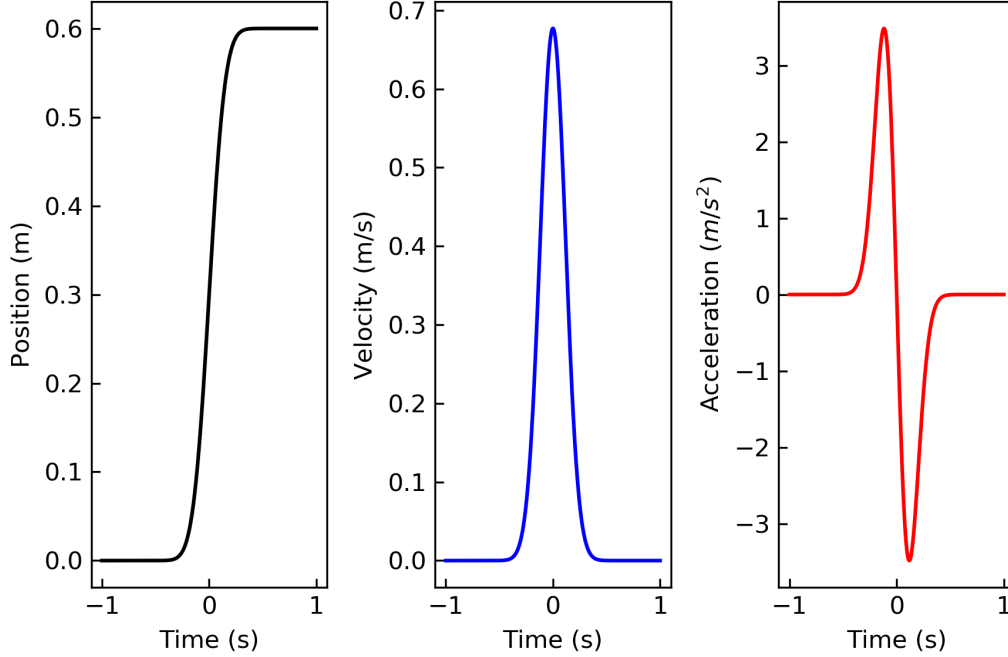


Figure 4.4: Error function trap position (left) described by equation (4.16), Gaussian velocity (centre) described by equation (4.17), and acceleration (right) as described by equation (4.18).

The Fourier transform for the Gaussian velocity is also Gaussian, and we expect the amplitude of oscillations to follow:

$$A(t_f) = F_f e^{(\frac{-\omega_z t_f}{12})^2}. \quad (4.19)$$

The simulation results for the Gaussian velocity profile are shown in figure 4.5. For times greater than 6.5 seconds the temperature change is less than the trap depth of 100 μK , therefore we would have to perform the transport over a minimum of 6.5 seconds if we choose to use this scheme.

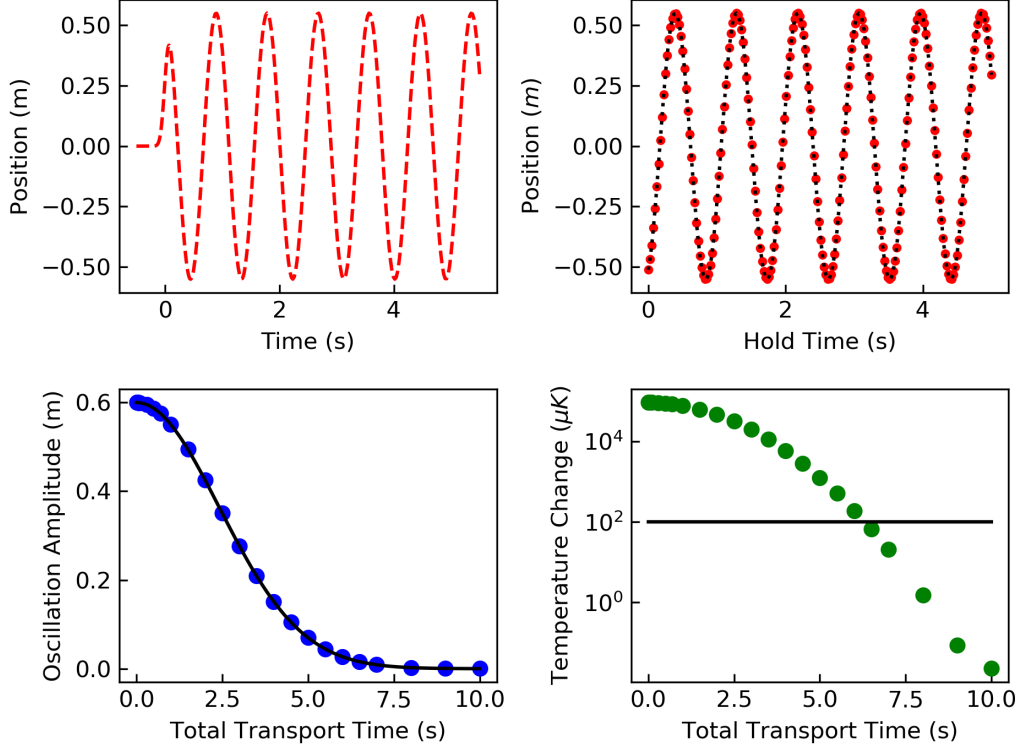


Figure 4.5: Results for transport with a Gaussian velocity profile. Top left: Sample plot of the position of the cloud of atoms with respect to the centre of the trap vs. time when the transport occurs over 1 second following which the atoms oscillate in a stationary trap for 5 seconds. Top right: Sample plot of atom position with respect to the center of the stationary trap vs. “hold” time since the transport period finished. Hold time defines the 5 seconds after the trap stopped moving. The position is fit to equation (4.14). Red dots are the data from the simulation, and the black dashed line is the fit. The fit parameters are: $A = -0.550634 \pm 3 \times 10^{-6}$, $B = 7.037168 \pm 3 \times 10^{-6}$, $C = 1.15713 \pm 1 \times 10^{-5}$, and $D = (-0.5 \pm 2) \times 10^{-6}$. Bottom left: Amplitude of the cloud oscillations vs. transport duration. The amplitude is the amplitude of the sine-wave fit from each transport time. Simulation data is shown by the blue dots, and the theoretically expected value is shown with the black line. Bottom right: Temperature change expected for each transport duration, calculated based off the oscillation amplitude. The black line shows the trap depth.

Triangular Velocity Profile

In this case, the velocity profile is a triangle, increasing with constant acceleration to a maximum at $t = \frac{t_f}{2}$ and then decreasing with constant acceleration until it reaches zero at $t = t_f$. The position, velocity, and acceleration are shown in figure 4.6 and are described by:

$$z_c(t) = \begin{cases} \frac{1}{2}a_t t^2 & 0 \leq t \leq \frac{t_f}{2} \\ \frac{1}{2}a_t \left(\frac{t_f}{2}\right)^2 + a_t \frac{t_f}{2} \left(t - \frac{t_f}{2}\right) - \frac{1}{2}a_t \left(t - \frac{t_f}{2}\right)^2 & \frac{t_f}{2} < t \leq t_f \end{cases} \quad (4.20)$$

$$\dot{z}_c(t) = \begin{cases} a_t t & 0 \leq t \leq \frac{t_f}{2} \\ a_t \frac{t_f}{2} - a_t \left(t - \frac{t_f}{2}\right) & \frac{t_f}{2} < t \leq t_f \end{cases} \quad (4.21)$$

$$\ddot{z}_c(t) = \begin{cases} a_t & 0 \leq t \leq \frac{t_f}{2} \\ -a_t & \frac{t_f}{2} < t \leq t_f \end{cases} \quad (4.22)$$

where t_f is the transport duration for a distance $d = 60$ cm, and $a_t = \frac{4d}{t_f^2}$.

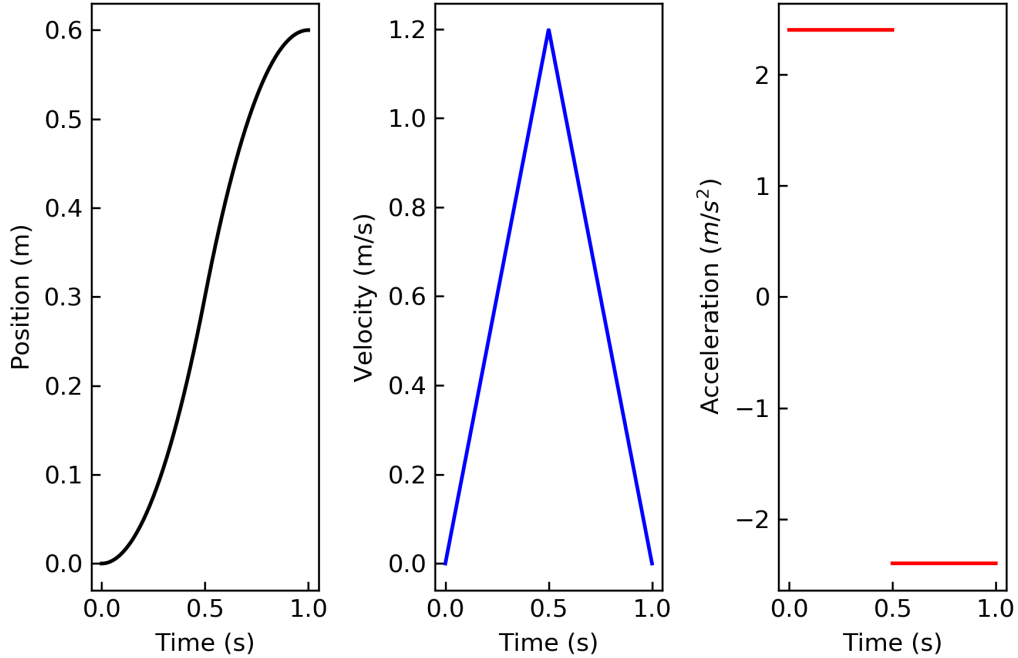


Figure 4.6: Quadratic trap position (left) as described by equation (4.20), triangular velocity (centre) as described by equation (4.21), and step function acceleration (right) as described by equation (4.22).

In this case the Fourier transform of the velocity is the sinc function, and the amplitude of oscillations is given by:

$$A(t_f) = d \operatorname{sinc}^2\left(\frac{\omega_z t_f}{4}\right), \quad (4.23)$$

where $\operatorname{sinc}(x) = \frac{\sin(x)}{x}$.

The results from the simulation are shown in figure 4.7. In this case, the oscillation amplitude, and thus the temperature increase, are zero whenever $\operatorname{sinc}^2\left(\frac{\omega_z t}{4}\right)$ is zero. Zeros occur at multiples of $2T = \frac{4\pi}{\omega_z}$, and after the second zero all transport durations give a temperature increase below the trap depth. For this scheme, the minimum transport time is $\frac{4\pi}{2\pi\omega_z} = 1.7857$ s. As our equipment has millisecond timing certainty, we should be able to come close enough to this time and keep heating to a minimum.

Sine-Squared Velocity Profile

In this scheme, the velocity follow a $\sin^2(t)$ shape between 0 and t_f , and is zero elsewhere. A plot is shown in figure 4.8. The position, velocity, and acceleration as a function of time are described by:

$$z_c(t) = \begin{cases} 0 & t < 0 \\ \frac{2d}{t_f} \left[\frac{t}{2} - \frac{t_f \sin\left(\frac{2\pi t}{t_f}\right)}{4\pi} \right] & 0 < t \leq t_f \\ d & t > t_f \end{cases} \quad (4.24)$$

$$\dot{z}_c(t) = \begin{cases} \frac{2d}{t_f} \sin^2\left(\frac{\pi t}{t_f}\right) & 0 \leq t \leq t_f \\ 0 & \text{otherwise} \end{cases} \quad (4.25)$$

$$\ddot{z}_c(t) = \begin{cases} \frac{2\pi d}{t_f^2} \sin\left(\frac{2\pi t}{t_f}\right) & 0 \leq t \leq t_f \\ 0 & \text{otherwise} \end{cases} \quad (4.26)$$

The oscillation amplitude is given by:

$$A(t_f) = \left| \frac{8d\pi^2}{t_f} \frac{\sin\left(\frac{\omega_z t_f}{2}\right)}{2\pi\omega_z - t_f^2\omega_z^3} \right|, \quad (4.27)$$

however due to singularities at $t_f = 0$ and $t_f = \sqrt{\frac{4\pi}{\omega_z^2}}$ it “blows up” for times less than 1 s. This function is zero when $\sin\left(\frac{\omega_z t_f}{2}\right) = 0$, when $\frac{\omega_z t_f}{2} = \pi$ except at the first zero, which is too close to a singularity. The results from

Velocity	Minimum transport duration (s)	Expected heating (μK)
Gaussian	6.5	66.41 ± 0.02
Triangular	1.8	0.0135 ± 0.0004
Sine squared	1.8	4.890 ± 0.006

Table 4.1: Table summarizing the minimum transport times required for each velocity profile.

this simulation are shown in figure 4.9. For transport duration greater than 1.7 seconds the temperature increase is below the trap depth, however until about 1.8 seconds (the second zero of $\sin(\frac{\omega_z t_f}{2})$) the temperature change is fairly close to the trap depth, and as vibrations from the equipment are likely to add additional heating, we will have to wait the same amount of time as with the triangular velocity profile.

Summary

Table 4.1 summarizes the minimum transport duration needed to keep the heating below the trap depth. Based on the simulation results, the triangular velocity profile will be the best for our set up as it minimizes the time we will need to wait in order to replenish the supply of atoms. Although the sine-squared profile has the same minimum transport duration the temperature increase, while below the trap depth, is greater than for the triangular velocity. As we expect additional heating due to equipment instability the option with the smallest temperature increase is the most desirable.

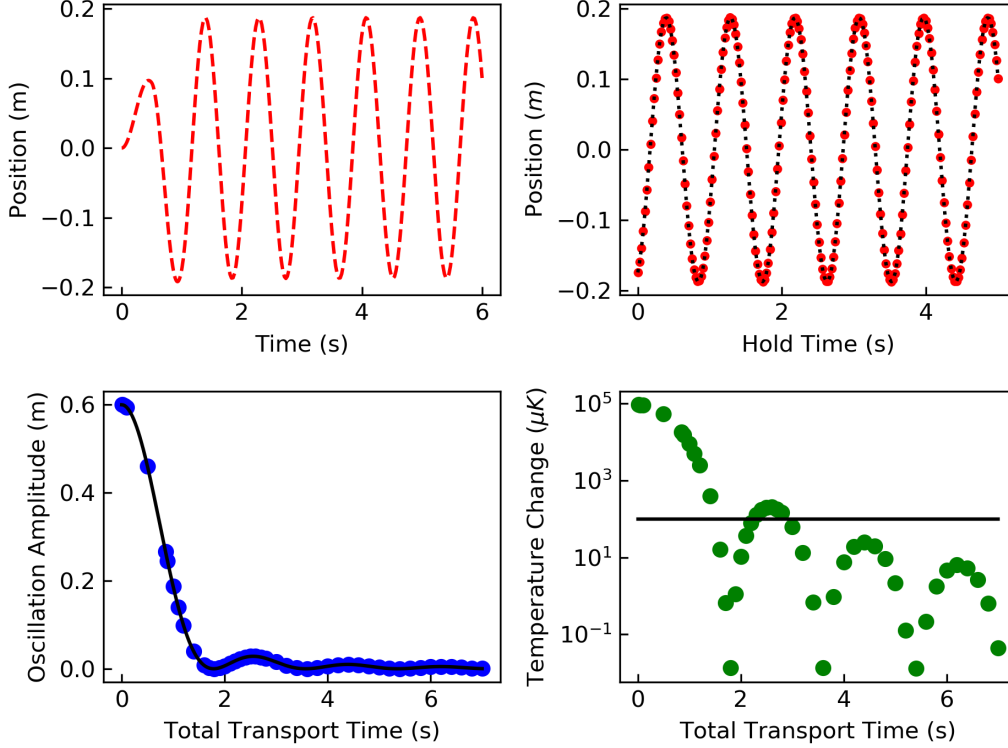


Figure 4.7: Triangular velocity profile results. Top left: Sample plot of the position of the cloud of atoms with respect to the centre of the trap vs. time when the transport occurs over 1 second following which the atoms oscillate in a stationary trap for 5 seconds. Top right: Sample plot of atom position with respect to the center of the stationary trap vs. “hold” time since the transport period finished. Hold time defines the 5 seconds after the trap stopped moving. The position is fit to equation (4.14). Red dots are the data from the simulation, and the black dashed line is the fit. The fit parameters are: $A = 0.187111 \pm 3 \times 10^{-6}$, $B = 7.03717 \pm 1 \times 10^{-5}$, $C = 1.94896 \pm 4 \times 10^{-5}$, and $D = (-0.4 \pm 2) \times 10^{-6}$. Bottom left: Amplitude of the cloud oscillations vs. transport duration. The amplitude is the amplitude of the sine-wave fit for each transport time. Simulation data is shown by the blue dots, and the theoretically expected value is shown with the black line. Bottom right: Temperature change, calculated based off of the oscillation amplitude, expected for each transport duration. The black line shows the trap depth.

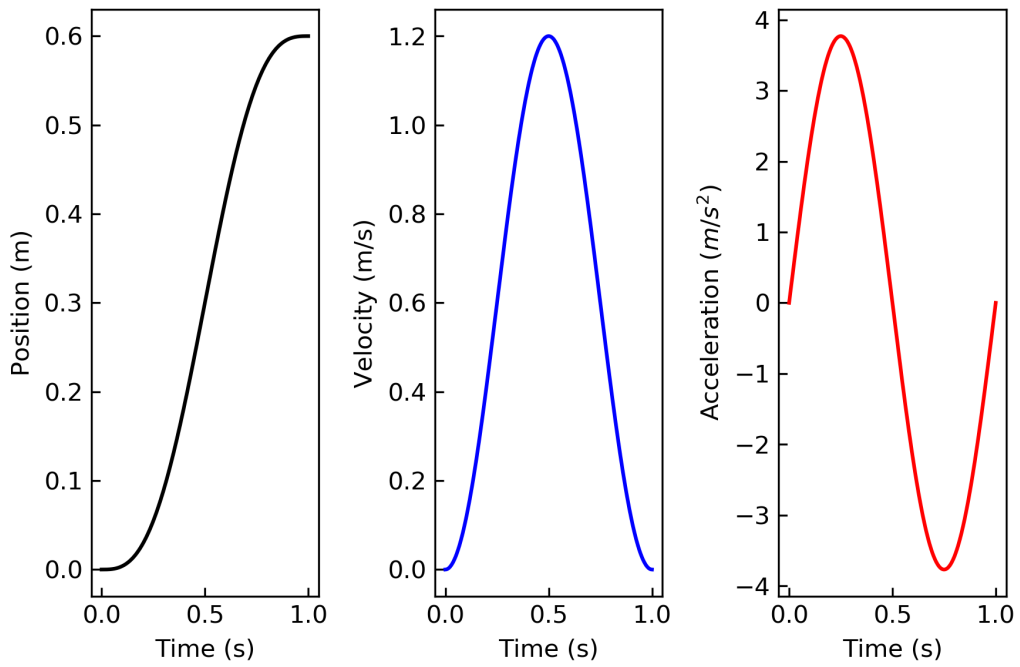


Figure 4.8: Sinusoidal trap position (left) as described by equation (4.24), velocity (centre) as described by equation (4.25), and acceleration (right) as described by equation (4.26).

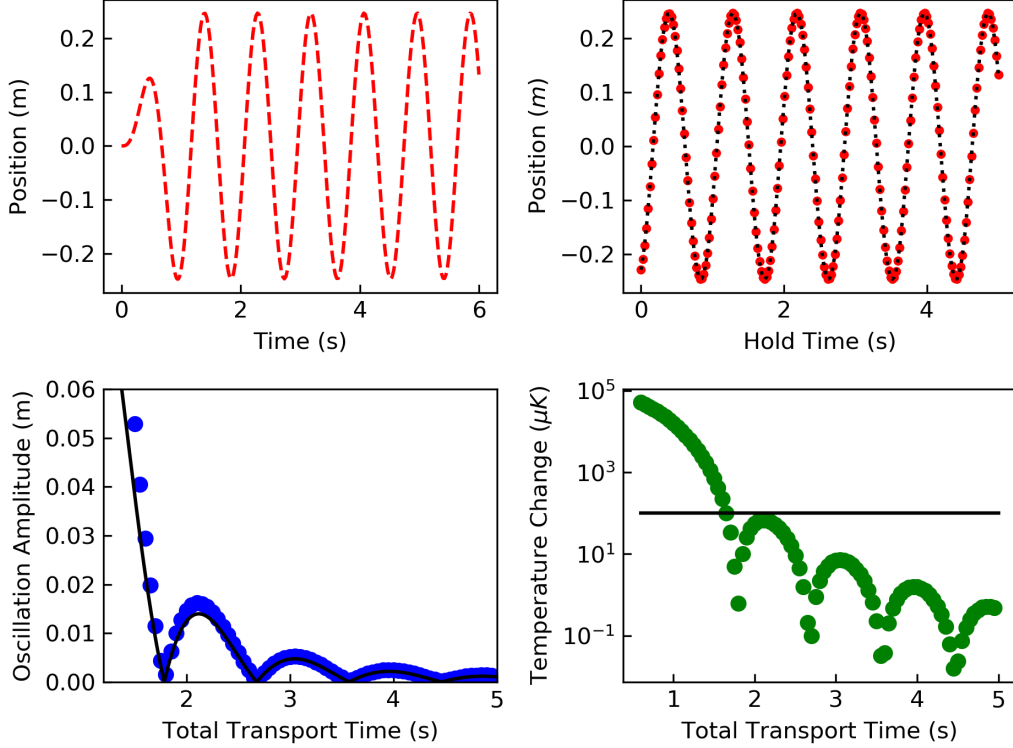


Figure 4.9: Results when velocity follows a sin squared profile. Top left: Sample plot of the position of the cloud of atoms with respect to the centre of the trap vs. time when the transport occurs over 1 second following which the atoms oscillate in a stationary trap for 5 seconds. Top right: Sample plot of atom position with respect to the center of the stationary trap vs. “hold” time since the transport period finished. Hold time defines the 5 seconds after the trap stopped moving. The position is fit to equation (4.14). Red dots are the data from the simulation, and the black dashed line is the fit. The fit parameters are: $A = 0.246816 \pm 3 \times 10^{-6}$, $B = 7.037169 \pm 7 \times 10^{-6}$, $C = 1.94866 \pm 3 \times 10^{-5}$, and $D = (-0.5 \pm 2) \times 10^{-6}$. Bottom left: Amplitude of the cloud oscillations vs. transport duration. The amplitude is the amplitude of the sine-wave fit for each transport time. Simulation data is shown by the blue dots, and the theoretically expected value is shown with the black line. Bottom right: Temperature change, calculated based off of the oscillation amplitude, expected for each transport duration. The black line shows the trap depth.

Chapter 5

Conclusion

In conclusion, I have designed a new apparatus which will combine laser-cooled atoms and cryogenically-cooled quantum devices. This apparatus consists of two parts: a UHV system used to laser cool ^{87}Rb atoms and a dilution fridge. Construction of the UHV system is complete, and it has been prepared for baking. In addition, the repump and cooling optics are set up and aligned. Coils for the MOT and magnetic trapping stages, as well as bias coils, have been wound, and we are awaiting custom machined mounts that will be used to align the coils to the apparatus. Once these parts are finished, and baking is complete, we can begin to cool the atoms. The dilution fridge is currently being manufactured.

We wish to couple the cold atoms to devices that are kept cool in the dilution fridge. This requires that atoms be moved approximately 60 cm from the centre of the cooling chamber into the fridge. A simulation of this process shows that a triangular velocity profile will allow the atoms to travel this distance in 1.8 s seconds while keeping heating below the trap depth, thus minimizing atom loss.

Much work remains in this project. We have yet to bake our UHV system, a step which precedes laser cooling the atoms. When the dilution fridge arrives, the construction can be completed. Although we have worked out the theory behind atom transport, implementation will be a further challenge. Once the

apparatus is functioning it will be used to study cold atom/ cryogenic hybrid quantum systems. Possible experiments are still in the preliminary planning stages, but they include quantum memory using atoms in a microwave cavity, coupling atoms to mechanical resonators or superconducting qubits for the purpose of state transfer, and experiments where quantum states are transferred to and stored in the atoms.

Bibliography

- [1] Richard P Feynman. Simulating physics with computers. *Int. J. Theor. Phys*, 21(6/7), 1982.
- [2] Peter W Shor. Algorithms for quantum computation: discrete logarithms and factoring. In *Proceedings 35th annual symposium on foundations of computer science*, pages 124–134. Ieee, 1994.
- [3] Edwin Pednault, John Gunnels, Dimitri Maslov, and Jay Gambetta. On “quantum supremacy”, 2019.
- [4] Edwin Pednault, John A. Gunnels, Giacomo Nannicini, Lior Horesh, and Robert Wisnieff. Leveraging secondary storage to simulate deep 54-qubit sycamore circuits, 2019.
- [5] Frank Arute, Kunal Arya, Ryan Babbush, Dave Bacon, Joseph C Bardin, Rami Barends, Rupak Biswas, Sergio Boixo, Fernando GSL Brandao, David A Buell, et al. Quantum supremacy using a programmable superconducting processor. *Nature*, 574(7779):505–510, 2019.
- [6] Yudong Cao, Jhonathan Romero, and Alán Aspuru-Guzik. Potential of quantum computing for drug discovery. *IBM Journal of Research and Development*, 62(6):6–1, 2018.
- [7] Federico Carminati. Viewpoint : Quantum thinking required. *CERN Courier*, 58(9):5–6, Oct 2018.
- [8] Seth Lloyd Bobak Toussi Kiani, Agnes Villanyi. Quantum medical imaging algorithms. Technical Report arXiv:2004.02036v1 [quant-ph], ArXiv, April 2020.

- [9] Florian Neukart, Gabriele Compostella, Christian Seidel, David Von Dollen, Sheir Yarkoni, and Bob Parney. Traffic flow optimization using a quantum annealer. *Frontiers in ICT*, 4:29, 2017.
- [10] Alejandro Perdomo-Ortiz, Neil Dickson, Marshall Drew-Brook, Geordie Rose, and Alán Aspuru-Guzik. Finding low-energy conformations of lattice protein models by quantum annealing. *Scientific reports*, 2:571, 2012.
- [11] H Jeff Kimble. The quantum internet. *Nature*, 453(7198):1023–1030, 2008.
- [12] David P DiVincenzo. The physical implementation of quantum computation. *Fortschritte der Physik: Progress of Physics*, 48(9-11):771–783, 2000.
- [13] Juan J García-Ripoll, Peter Zoller, and J Ignacio Cirac. Quantum information processing with cold atoms and trapped ions. *Journal of Physics B: Atomic, Molecular and Optical Physics*, 38(9):S567, 2005.
- [14] Göran Wendin. Quantum information processing with superconducting circuits: a review. *Reports on Progress in Physics*, 80(10):106001, 2017.
- [15] Markus Aspelmeyer, Simon Gröblacher, Klemens Hammerer, and Nikolai Kiesel. Quantum optomechanics—throwing a glance. *JOSA B*, 27(6):A189–A197, 2010.
- [16] E Jané, MB Plenio, and D Jonathan. Quantum-information processing in strongly detuned optical cavities. *Physical Review A*, 65(5):050302, 2002.
- [17] Michael N Leuenberger, Daniel Loss, Martino Poggio, and David D Awschalom. Quantum information processing with large nuclear spins in gaas semiconductors. *Physical review letters*, 89(20):207601, 2002.
- [18] Filippo Troiani, Ulrich Hohenester, and Elisa Molinari. Exploiting exciton-exciton interactions in semiconductor quantum dots for quantum-information processing. *Physical Review B*, 62(4):R2263, 2000.

- [19] Gershon Kurizki, Patrice Bertet, Yuimaru Kubo, Klaus Mølmer, David Petrosyan, Peter Rabl, and Jörg Schmiedmayer. Quantum technologies with hybrid systems. *Proceedings of the National Academy of Sciences*, 112(13):3866–3873, 2015.
- [20] David Petrosyan, Guy Bensky, Gershon Kurizki, Igor Mazets, Johannes Majer, and Jörg Schmiedmayer. Reversible state transfer between superconducting qubits and atomic ensembles. *Physical Review A*, 79(4):040304, 2009.
- [21] P Weiss, M Knufinke, S Bernon, D Bothner, L Sárkány, C Zimmermann, R Kleiner, D Koelle, J Fortágh, and H Hattermann. Sensitivity of ultracold atoms to quantized flux in a superconducting ring. *Physical review letters*, 114(11):113003, 2015.
- [22] J Verdú, H Zoubi, Ch Koller, J Majer, H Ritsch, and J Schmiedmayer. Strong magnetic coupling of an ultracold gas to a superconducting waveguide cavity. *Physical review letters*, 103(4):043603, 2009.
- [23] H Hattermann, D Bothner, LY Ley, B Ferdinand, D Wiedmaier, L Sárkány, Reinhold Kleiner, Dieter Koelle, and J Fortágh. Coupling ultracold atoms to a superconducting coplanar waveguide resonator. *Nature communications*, 8(1):1–7, 2017.
- [24] Matthew A Naides, Richard W Turner, Ruby A Lai, Jack M DiSciaccia, and Benjamin L Lev. Trapping ultracold gases near cryogenic materials with rapid reconfigurability. *Applied Physics Letters*, 103(25):251112, 2013.
- [25] Stefan Minniberger, Fritz Diorico, Stefan Haslinger, Christoph Hufnagel, Christian Novotny, Nils Lippok, Johannes Majer, Christian Koller, Stephan Schneider, and Jörg Schmiedmayer. Magnetic conveyor belt transport of ultracold atoms to a superconducting atomchip. *Applied Physics B*, 116(4):1017–1021, 2014.

- [26] Florian Jessen, Martin Knufinke, SC Bell, Petra Vergien, Helge Hattermann, Patrizia Weiss, Matthias Rudolph, M Reinschmidt, K Meyer, Tobias Gaber, et al. Trapping of ultracold atoms in a $3\text{He}/4\text{He}$ dilution refrigerator. *Applied Physics B*, 116(3):665–671, 2014.
- [27] Alessandro Landra, Christoph Hufnagel, Lim Chin Chean, Thomas Weigner, Yung Szen Yap, Long Hoang Nguyen, and Rainer Dumke. Design of an experimental platform for hybridization of atomic and superconducting quantum systems. *Physical Review A*, 99(5):053421, 2019.
- [28] Hai Zhong, Gotthold Fläschner, Alexander Schwarz, Roland Wiesendanger, Philipp Christoph, Tobias Wagner, Andreas Bick, Christina Staarman, Benjamin Abeln, Klaus Sengstock, et al. A millikelvin all-fiber cavity optomechanical apparatus for merging with ultra-cold atoms in a hybrid quantum system. *Review of Scientific Instruments*, 88(2):023115, 2017.
- [29] Philipp Christoph, Tobias Wagner, Hai Zhong, Roland Wiesendanger, Klaus Sengstock, Alexander Schwarz, and Christoph Becker. Combined feedback and sympathetic cooling of a mechanical oscillator coupled to ultracold atoms. *New Journal of Physics*, 20(9):093020, 2018.
- [30] C.J. Foot. *Atomic physics*. Oxford master series in physics. Oxford University Press, 2005.
- [31] Theodor W Hänsch and Arthur L Schawlow. Cooling of gases by laser radiation. *Optics Communications*, 13(1):68–69, 1975.
- [32] D Steck. Rb 87 d line data, 2006.
- [33] Paul D Lett, Richard N Watts, Christoph I Westbrook, William D Phillips, Phillip L Gould, and Harold J Metcalf. Observation of atoms laser cooled below the doppler limit. *Physical review letters*, 61(2):169, 1988.

- [34] Jean Dalibard and Claude Cohen-Tannoudji. Laser cooling below the doppler limit by polarization gradients: simple theoretical models. *JOSA B*, 6(11):2023–2045, 1989.
- [35] EL Raab, M Prentiss, Alex Cable, Steven Chu, and David E Pritchard. Trapping of neutral sodium atoms with radiation pressure. *Physical Review Letters*, 59(23):2631, 1987.
- [36] Rudolf Grimm, Matthias Weidemüller, and Yurii B Ovchinnikov. Optical dipole traps for neutral atoms. *Advances In Atomic, Molecular, and Optical Physics*.
- [37] CR Monroe, Eric A Cornell, CA Sackett, CJ Myatt, and CE Wieman. Measurement of cs-cs elastic scattering at $t= 30 \mu\text{k}$. *Physical review letters*, 70(4):414, 1993.
- [38] H.J. Metcalf and P. van der Straten. *Laser Cooling and Trapping*. Graduate Texts in Contemporary Physics. Springer New York, 2001.
- [39] MD Barrett, JA Sauer, and MS Chapman. All-optical formation of an atomic bose-einstein condensate. *Physical Review Letters*, 87(1):010404, 2001.
- [40] Kurt J. Lesker Company. Cf flanges technical notes, 2020.
- [41] Stefan Schmid, Gregor Thalhammer, Klaus Winkler, Florian Lang, and Johannes Hecker Denschlag. Long distance transport of ultracold atoms using a 1d optical lattice. *New Journal of Physics*, 8(8):159, 2006.
- [42] Markus Greiner, Immanuel Bloch, Theodor W Hänsch, and Tilman Esslinger. Magnetic transport of trapped cold atoms over a large distance. *Physical Review A*, 63(3):031401, 2001.
- [43] AP Chikkatur, Y Shin, AE Leanhardt, D Kielpinski, E Tsikata, TL Gustavson, DE Pritchard, and W Ketterle. A continuous source of bose-einstein condensed atoms. *Science*, 296(5576):2193–2195, 2002.

- [44] Julian Léonard, Moonjoo Lee, Andrea Morales, Thomas M Karg, Tilman Esslinger, and Tobias Donner. Optical transport and manipulation of an ultracold atomic cloud using focus-tunable lenses. *New Journal of Physics*, 16(9):093028, 2014.
- [45] Emanuel Paul Berger. An aberration-corrected high resolution imaging system for ultracold atoms . Master's thesis, ETH Zurich, Switzerland, 2017.
- [46] Antoine Couvert, T Kawalec, G Reinaudi, and David Guéry-Odelin. Optimal transport of ultracold atoms in the non-adiabatic regime. *EPL (Europhysics Letters)*, 83(1):13001, 2008.

Appendix A

Focus Tunable Lens Transport Code

This code calculates the position and size of the beam waist once a colimated beam has passed through the focus tunable lens, and a fixed focal length lens.

```
#!/usr/bin/env python3
# -*- coding: utf-8 -*-
"""
Created on Tue Feb 11 09:56:12 2020

@author: MichelleSullivan

Code to calculate the beam size at a given position
after the lens. It will show
beam size vs. position as well as printing out the focus
radius and position.
"""

import numpy as np
import matplotlib.pyplot as plt
import math as math

#Wavelength of the light we are using
WaveLength = 1064e-9 #in m

w_0 = 2.5e-3 #Radius of the beam colimated by the first
two lens, in m
f_3 = 500e-3 #focal length of the 3rd finxed len in m (
lens after the tunable lens)
d_2 = f_3 #the distance between the tunable lens and the
focusing lens is fixed to keep beam wasit constant
```

```

d_3 = np.linspace(0,1200e-3,1000) #array of distances
    measured with respect to the last lens
f_T = 1/0.65#focal length of tunable lens, in m

#Create the system ABCD matrix which represents a
    collimated beam
#travelling through the tunable lens, a distance d_2, a
    focusing lens f_3
#followed by a distance d_3. These values must be input.
    Will return ABCD matrix for entire system
def ABCD_sys(f_T, d_2, f_3, d_3):
    M_00 = (f_3*f_T-d_3*f_T+d_2*f_3+d_2*d_3-d_3*f_3)/(
        f_3*f_T)
    M_01 = (d_2*f_3-d_2*d_3+d_3*f_3)/f_3
    M_10 = (d_2-f_3-f_T)/(f_3*f_T)
    M_11 = (f_3-d_2)/f_3
    return np.array([[M_00,M_01],[M_10,M_11]])

#Calcualte z_R (rayleigh range) given w_0
#input:
    #w_0 beam waist in meters
    #wavelength of the light in meters
#Function returns the rayleigh range in meters
def Rayleigh(w_0, wavelength):
    z_R = (np.pi*w_0**2)/wavelength
    return z_R

#Calculate the complex beam parameter given the radius
    of curvature, R (in meters),
#and the rayleigh range, z_R (in meters). The function
    returns
#the complex number 1/q_i in m^-1
def complex_initial(R, z_R):
    q_i_inv = 1/R - 1j/z_R
    return q_i_inv

#Calculate the final complex beam parameter given the
    ABCD matrix after propagation
#Input:
    #q_i initial complex beam parameter
    #M_sys ABCD matrix for the system, after bema has
        been traced
#returns 1/q_f = 1/R_f - i/z_Rf
def complex_final(q_i, M_sys):
    A = M_sys[0,0]

```

```

    B = M_sys[0,1]
    C = M_sys[1,0]
    D = M_sys[1,1]
    q_f_inv = (C+D/q_i)/(A+B/q_i)
    return q_f_inv

#Calculate w_0 given the rayleigh range
#input:
    #z_R rayleigh range in meters
    #wavelength of light in meters
#Function returns w_0 in meters
def waist(z_R, wavelength):
    w_0 = np.sqrt((wavelength*z_R)/np.pi)
    return w_0

#Complex beam parameter for intial collimated beam
z_Ri = Rayleigh(w_0, WaveLength) #calculate rayleigh
    range
R_i = math.inf #beam radius of curvature
q_i_inv = complex_initial(R_i,z_Ri)

w = np.zeros(len(d_3)) #empty array to store waist sizes
for i in range(len(d_3)): #loops through all distances
    in d_3 and calculate waist
    M_sys = ABCD_sys(f_T, d_2, f_3, d_3[i])
    q_f_inv = complex_final(1/q_i_inv, M_sys)
    z_Rf = -1/q_f_inv.imag
    w_test = waist(z_Rf, WaveLength)
    w[i] = w_test #save wasit size
#print(w)

#Make a nice plot showing the beam size vs. position.
    Include both 1/e^2 and 99% of power
plt.plot(d_3, w*1e3, 'r', label = '1/e^2_waist')
plt.plot(d_3, -w*1e3, 'r')
#plt.plot(d_3, 2*w*1e3, 'k--', label = '99% of power')
#plt.plot(d_3, -2*w*1e3, 'k--')
plt.rcParams['xtick.direction'] = 'in'
plt.rcParams['ytick.direction'] = 'in'
plt.grid()
plt.xlabel('Distance_From_Final_Lens_(m)')
plt.ylabel('Beam_size_(mm)')
#plt.legend()
plt.show()

```

```
waist_size = np.amin(w) #Find the minimum waist size
waist_loc = d_3[np.argmin(w)] #Minimum waist location
#print results
print('The focus radius is ', waist_size*1e6, ' microns.')
print('The waist is ', waist_loc*1e3, ' mm away from the
      final lens.')
```

Appendix B

Atom Distribution Generation Code

This code generates a cloud of atoms with normally distributed z-position and momentum.

```
# -*- coding: utf-8 -*-
"""
Code to generate normally distributed atom positions and
velocities in the z coordinate.
Code will generate the distribution, fit it to a normal
distribution to extract temperature,
plot the results, and save the coordinates in CSV file.
"""

import numpy as np
import matplotlib.pyplot as plt
from scipy.optimize import curve_fit

#Define constants
omega_z = 2*np.pi*1.12
Temp = 30e-6
k_b = 1.38e-23
mass = 1.44e-25

#Function to fit the position distribution and extract
temperature and mean
def position_z(z, t, mu_z):
    K = np.sqrt((mass*omega_z**2)/(2*k_b*t))
    return K/np.sqrt(np.pi)*np.exp(-K**2*(z-mu_z)**2)

#function to fit momentum distribution and extract
temperature and mean
```

```

def dist_pz(pz, t):
    C = 2*mass*k_b*t
    return np.sqrt(1/(C*np.pi))*np.exp(-(pz)**2/C)

#Define number of atoms
npoints = 10000
#Define number of bins in histogram
nbins = 100

#Standard deviation for position and momentum, to be
    used when
#assigning random pos and mommoentum to the atoms
sigma_z = np.sqrt(k_b*Temp/(mass*omega_z**2))
sigma_p = np.sqrt(mass*k_b*Temp)
#Generate a random normal distribution of atom positions
    and momentums
z_dis = np.random.randn(npoints)*sigma_z
pz_dis = np.random.randn(npoints)*sigma_p
#save the data
np.savetxt('atom_coordiantes_zonly.csv', (z_dis, pz_dis),
    delimiter = ',')

#Make a histogram of atom position

plt.figure(1)
hist_z, bins_z, patches_z = plt.hist(z_dis, nbins,
    density = True)
plt.title('$Z$')

#make a histogram of atom momentum
plt.figure(2)
hist_pz, bins_pz, patches_pz = plt.hist(pz_dis, nbins,
    density = True)
plt.title('$P_z$')

#Find the centre of each bin
bincenters_z = np.array([0.5*(bins_z[i]+bins_z[i+1]) for
    i in range(len(bins_z)-1)])
#fit the data to the function defined above, extract
    temperature and mean
fit_params, fit_cov = curve_fit(position_z, bincenters_z
    , hist_z, [Temp,0])

#Find centre of momentum bins

```

```

bincenters_pz = np.array([0.5*(bins_pz[i]+bins_pz[i+1])
    for i in range(len(bins_pz)-1)])
#Fit the distribution to the function defined above,
    extract temperature
fit_params_p, fit_cov_p = curve_fit(dist_pz,
    bincenters_pz, hist_pz, [Temp])

#Add the fit to the histograms
plt.figure(1)
fit = np.linspace(-5*sigma_z, 5*sigma_z, 1000)
plt.plot(fit, position_z(fit, *fit_params))

plt.figure(2)
fit_pz = np.linspace(-5*sigma_p, 5*sigma_p, 1000)
plt.plot(fit_pz, dist_pz(fit_pz, *fit_params_p) )

#Extract desired values from the fit and print them out
T_z_fit = fit_params[0]*1e6
T_z_unc = np.sqrt(fit_cov[0,0])*1e6

z_cen = fit_params[1]*1e6
z_cen_unc = np.sqrt(fit_cov[1,1])*1e6

print("Temperature_from_fit = ", T_z_fit, '+/-', T_z_unc
    , 'microkelvin.')
print('The_cener_of_the_distribution_is_at', z_cen, '+/-'
    , z_cen_unc, 'microns.')

T_pz_fit = fit_params_p[0]*1e6
T_pz_unc = np.sqrt(fit_cov_p[0,0])*1e6

print("Temperature_from_momentum_fit_is", T_pz_fit, "+/-"
    , T_pz_unc)

#Make a nice final figure, which shows position and
    momentum side by side

plt.figure(3)
fig, axs = plt.subplots(1,2, tight_layout = True)

N1, bins1, patches1 = axs[0].hist(z_dis, nbins, density
    = True, color = 'b', label = 'Distrubution')
axs[0].plot(fit, position_z(fit, *fit_params), '-k')
axs[0].set_title('Position')
axs[0].set_xlabel('z_(m)')

```

```
axs[0].set_ylabel('Normalized_Density')
axs[0].tick_params(direction = 'in')

N2, bins2, patches2 = axs[1].hist(pz_dis, nbins, density
    = True, color = 'r')
axs[1].plot(fit_pz, dist_pz(fit_pz, *fit_params_p), '-k')
axs[1].set_title('Momentum')
axs[1].set_xlabel(r'$p_z$(kg_m/s)')
axs[1].tick_params(direction = 'in')
```

Appendix C

Atom Transport Simulation Code

Below is the code used in the atom transport simulation. The user can select an acceleration profile by un-commenting it in the code, and can input an array of total transport times. The code then use the python function “odeint” to integrate the equations of motion for each atom. At each time step the distribution is fit to a Gaussian function to extract the distribution center. The distribution vs. center data is fit to a sine function, which extracts the amplitude of oscillations. This is repeated for each total transport time, and plots of oscillation amplitude vs. total transport time and temperature change vs. total transport time are made.

```
"""
```

```
This code has three different acceleration profiles . .  
Uncomment the one you  
wish to use .
```

```
This code integrates the equations of motion at each  
time point , for each atom .  
At each time step , it fits the distribution to determine  
the distribution center ,  
and extract a temperature from the fit .
```

```
The transport will take place over a period " t_final " . .  
In this version of the code ,  
a loop will carry out the process for an array of "  
t_final " values . . After that ,  
the atoms remain in a stationary trap for a period '  
t_wait ' . . The center position of the
```

cloud will oscillate around the trap center. The position from this portion of the motion is fit to a sine wave in order to extract amplitude and frequency. Two plots are more. One shows the amplitude change along with the theory expectation, the other shows the temperature change with a log scale on the y-axis.

Data is imported from a csv file. I use the distribution generated with the script 'Atom_Distribution_zony'

The parameters from the fit to the sine wave will be saved in a csv, along with uncertainty.

"""

```

import numpy as np
from scipy.integrate import odeint
import matplotlib.pyplot as plt
from scipy.optimize import curve_fit

#constants
omega_z = 2*np.pi*1.12
Temp = 30e-6
k_b = 1.38e-23
mass = 1.44e-25
#Standard deviation for position and momentum
sigma_z = np.sqrt(k_b*Temp/(mass*omega_z**2))
sigma_p = np.sqrt(mass*k_b*Temp)

#number of atoms and bins for histogram. Same as used
when generating
#the distribution
nbins = 100
natoms = 10000

#make an array of transport durations
t_final = np.arange(0.6,5,0.05)
#after the transport, wait for several oscillation
periods

```

```

t_wait = 5

#distance to transport over
d = 0.6

#times to be used when plotting the theory result
t_theory = np.linspace(0,max(t_final),500)
#result expected from theory
#theory = d*np.sinc(omega_z*t_theory/(4*np.pi))**2

#load the data
X = np.loadtxt('atom_coordiantes_zonly.csv', delimiter =
              ',')

#Define a sinwave to be used when fitting the "
stationary" position
def sinewave(t,A,B,C,D):
    return A*np.sin(B*t-C)+D

#Define trap position
#With waiting

#Acceleration for the sine^2 velocity.
def acceleration(t, t_f):
    if 0 <= t <= t_f:
        return ((2*np.pi*d)/t_f**2)*np.sin(2*np.pi*t/t_f
        )
    else:
        return 0
"""
#Acceleration for the triangular velocity
def acceleration(t, t_f):
    if 0 <= t <= t_f/2:
        return a_t
    elif t_f/2 < t <= t_f:
        return -a_t
    else:
        return 0

#acceleration for the gaussian velocity
def acceleration(t, t_f):
    if t < t_f:
        return v_trap(t)*(-72*t/t_f**2)
    else:

```

```

.....return _0
"""

#define ODEs. This includes trap motion

def transport(X, t, t_f):
    z, p_z = X
    dz = p_z/mass
    dpz = -mass*omega_z**2*z +mass*acceleration(t, t_f)
    return np.array([dz, dpz])

#Function to fit the position distribution and extract
temperature and mean
def position_z(z, t, mu_z):
    K = np.sqrt((mass*omega_z**2)/(2*k_b*t))
    return K/np.sqrt(np.pi)*np.exp(-K**2*(z-mu_z)**2)

#function to fit momentum distribution and extract
temperature and mean
def dist_pz(pz, t, mu_pz):
    C = 2*mass*k_b*t
    return np.sqrt(1/(C*np.pi))*np.exp(-(pz-mu_pz)**2/C)

#arrays to store coefficients from sine fit
A = np.zeros(len(t_final))
A_unc = np.zeros(len(t_final))
B = np.zeros(len(t_final))
B_unc = np.zeros(len(t_final))
C = np.zeros(len(t_final))
C_unc = np.zeros(len(t_final))
D = np.zeros(len(t_final))
D_unc = np.zeros(len(t_final))

for k in range(len(t_final)):
    #select the transport duration for this iteration
    t_total = t_final[k]+t_wait
    #integration times
    #Time where the trap is moving
    transport_time = np.linspace(0, t_final[k], 1000)
    #Time where the trap is stationary
    wait = np.linspace(t_final[k]+0.0001, t_total, 200 )
    #Total time
    wait_time = np.append(transport_time, wait)
    t_f = t_final[k]

```

```

#acceleration
a_t = (4*d)/t_f**2

#Array that will store the temperature and
    uncertainty at each integration step
wait_Temp = np.zeros(len(wait_time))
temp_unc = np.zeros(len(wait_time))
#Array to store dist centre and unc at each
    integration time step
wait_center = np.zeros(len(wait_time))
center_unc = np.zeros(len(wait_time))

#array to store the position solution for all atoms
    at all times
pos = np.zeros((len(wait_time), natoms))

#Solve the ODEs for each atom, store the position
    and momentum at each
#time step in a n array
for i in range(len(X[0])):

    t_f = t_final[k]
    solution = odeint(transport, X[:, i], wait_time,
        args = (t_f, ), rtol = 1e-10, atol = 1e-10)
    pos[:, i] = solution[:, 0]

#For each time step, fit the position distribution
for j in range(len(wait_time)):
    hist, bin_edges = np.histogram(pos[j, :], nbins,
        density = True)
    #Find bin centers and fit
    bincenters = np.array([0.5*(bin_edges[k]+
        bin_edges[k+1]) for k in range(len(bin_edges)
        -1)])
    mu_guess = np.mean(pos[j, :])
    fit_params, fit_cov = curve_fit(position_z,
        bincenters, hist, [Temp, mu_guess])
    wait_Temp[j] = fit_params[0]
    temp_unc[j] = np.sqrt(fit_cov[0, 0])
    wait_center[j] = fit_params[1]
    center_unc[j] = np.sqrt(fit_cov[1, 1])

#Data when the trap is stationary
time_sub = wait_time[1000:]

```

```

center_sub = wait_center[1000:]
#Fit a sine wave to this portion of the data
fit_params_sub, fit_cov_sub = curve_fit(sinewave,
    time_sub, center_sub, [max(center_sub), 2*np.pi
    *1.12, 1.5, 0])
time_fit_sub = np.linspace(t_final, t_total, 200)
sin_sub = sinewave(time_fit_sub, *fit_params_sub)
#Store the results
A[k] = fit_params_sub[0]
A_unc[k] = np.sqrt(fit_cov_sub[0,0])
B[k] = fit_params_sub[1]
B_unc[k] = np.sqrt(fit_cov_sub[1,1])
C[k] = fit_params_sub[2]
C_unc[k] = np.sqrt(fit_cov_sub[2,2])
D[k] = fit_params_sub[3]
D_unc[k] = np.sqrt(fit_cov_sub[3,3])

#save the times and the parameters from when the
    position vs. time data was fit
    #to a sin function
np.savetxt('sine2_velocity_results_2.csv', (t_final, A,
    A_unc, B, B_unc, C, C_unc, D, D_unc), delimiter = ',')

#plot amplitude vs. time
plt.figure(1)
plt.errorbar(t_final, abs(A), A_unc, linestyle = 'none')
plt.plot(t_final, A, 'bo', label = 'Simulation')
#plt.plot(t_theory, theory, 'k--', label = 'Theory')
plt.xlabel('Transport_Time_(s)')
plt.ylabel('Oscillation_Amplitude_(m)')
plt.tick_params(direction = 'in')
plt.legend()

#calculate the change in temperautre
T = (mass*omega_z**2*A**2)/(2*k_b)
T_max = np.ones(len(t_theory))*100
#Plot temperature change vs. time
plt.figure(2)
plt.plot(t_final, T*1e6, 'go', label = 'Simulation')
plt.plot(t_theory, T_max, 'k', label = 'Trap_Depth')
plt.xlabel('Transport_Time_(s)')
plt.ylabel(r'Temperautre_Change_($\mu_K$)')
plt.tick_params(direction = 'in')
plt.yscale('log')

```

```
plt.legend()
```